5-10-2019

SYNTHESIS AND PROPERTIES OF LIPOIC ACID STABILIZED GOLD NANOCLUSTERS

Minh Tri Tran
mtran41@student.gsu.edu

SYNTHESIS AND PROPERTIES OF LIPOIC ACID STABILIZED GOLD NANOCLUSTERS

by

MINH TRI HOANG TRAN

Under the Direction of Gangli Wang, PhD

ABSTRACT

Disulfide lipoic acid was used to synthesize new aqueous soluble gold nanomaterials. The first one is an ultra-small plasmonic nanoparticle displaying a weak plasmonic band at 520 nm. At the transition zone between larger metallic nanoparticles and smaller non-metallic nanoclusters, intriguing electrochemical and optical features were observed. The other cluster is a new molecular-like nanocluster with unique optical features. Distinct UV-visible absorption bands were observed corresponding to discrete energy states/orbitals along with a weak photoluminescence if ultracentrifuge purification is adopted. Dialysis purification yielded a tenfold increase in photoluminescence while the absorption bands diminish. This transition is attributed to the gradual oxidation of some of the sulfur atoms at the core-ligand interface. Annealing with a known amount of excess thiol is shown to expedite and better control the

transitions observed through the synthesis and purification along with yielding an enhancement of the electrochemiluminescence by more than ten folds.

INDEX WORDS: Gold nanoclusters, Surface plasmon resonance, Near-IR luminescence

SYNTHESIS AND PROPERTIES OF LIPOIC ACID STABILIZED GOLD NANOCLUSTERS

by

MINH TRI HOANG TRAN

A Thesis Submitted in Partial Fulfillment of the Requirements for the Degree of

Master of Science

in the College of Arts and Sciences

Georgia State University

2019

SYNTHESIS AND PROPERTIES OF LIPOIC ACID STABILIZED GOLD NANOCLUSTERS

by

MINH TRI HOANG TRAN

Committee Chair: Gangli Wang

Committee: Kathryn Grant

Gabor Patonay

Electronic Version Approved:

Office of Graduate Studies

College of Arts and Sciences

Georgia State University

May 2019

DEDICATION

I want to thank my father, Duc Minh Hoang Tran, and mother, Eve Annick Ho for their love and support.

ACKNOWLEDGEMENTS

Firstly, I would like to thank Dr. Gangli Wang for accepting me into his lab giving me the opportunity to work, learn and do research under his guidance. I also thank for all the support and advice he gave me. Secondly, I would like to thank every member of the Gangli Wang research group for everything that comes along with working as a team. I also want to acknowledge Dr. Tanyu Wang, Dr. Warren Brown, Dr. Jonathan W. Padelford, Marksim M. Kvetny, and Michael Bowen for their training and knowledge they gave me. I would like to thank Jonathan W. Padelford and Heidi Ma for helping me to run some of the experiments leading to the creation of this thesis. I also thank Dr. Zhenming Du for his assistance with NMR. Finally, I would like to thank many other GSU faculty for their advice and encouragement to pursue advanced study in the field of chemistry.

TABLE OF CONTENTS

ACKNOWLEDGEMENTS V

LIST OF TABLES IX

LIST OF FIGURES X

LIST OF ABBREVIATIONS XVIII

1 INTRODUCTION 1

1.1 Chemistry and Nanomaterials 1

1.2 Three-dimensional spherical Gold Nanomaterials 2

1.2.1 Plasmonic gold nanoparticles 4

1.2.2 Molecular-like gold nanoclusters 5

1.3 Roles of stabilizing ligands 7

1.4 Motivation 8

2 EMERGENCE OF SURFACE PLASMON RESONANCE: FROM GOLD NANOCLUSTERS TO NANOPARTICLES WITH MULTIDENTATE LIGANDS LIPOIC ACID 12

2.1 Abstract 12

2.2 Background and strategy 12

2.3 Experimental details 14

2.4 Results and Discussion 15

2.4.1 Changes in Plasmonic band intensity with the amount of lipoic acid in synthesis. 15

2.4.2 Optimization of synthesis based on spectroscopy monitoring 18

2.4.3 Electrochemical and optical properties of characteristic plasmonic gold nanoparticles 24

2.5 Conclusion 36

3 MOLECULAR-LIKE LIPOIC ACID STABILIZED GOLD NANOCLUSTERS 38

3.1 Abstract 38

3.2 Background and strategy 39

3.3 Experimental details 41

3.4 Results and Discussion 42

3.4.1 Gold Lipoic Acid nanoclusters synthesis process monitored by spectroscopy and parameter optimization 42

3.4.2 Optical features affected by different purification methods. 46

3.4.3 Impact on optical features by the variation of Lipoic acid ratios to Gold .. 49

3.4.4 Impacts on optical features by the variation of reductant ratio 50

3.4.5 Oxidized sulfur identified by Infrared spectroscopy 52

3.4.6 Ligand composition by NMR 55

3.4.7 Spectroelectrochemical analysis 58

3.4.8 Heat treatment to enhance photoluminescence. 63

3.5 Conclusion 75

4 SUMMARY 77

REFERENCES 79

APPENDICES 83

Appendix A: Chemicals 83

Appendix B: Instrumentation and Measurements 83

LIST OF TABLES

Table 2-1. Peaks and peak spacings in the oxidation and reduction scans of SWV and CV of Au-LA 1-0.39 in aqueous and organic; And 1-0.35 in aqueous. Red, Blue, and green colors represent the matching signals from the same potential or energy state..... 29

Table 2-2. peaks (black color) and valley (red color) position in 0.39 SP NPs Spectro electrochemistry panels..... 33

LIST OF FIGURES

Figure 1-1. Lipoic acid structure. 8

Figure 1-2. Basic representation of $Au_{22}LA_{12}$ nanocluster. Only two different ligand forms are sketched for clarity. The metal NCs are often described by unique compositions with discrete numbers of metal atoms and ligands. 9

Figure 2-1. Normalized absorbance spectra of different (reaction mixtures/products?) at the listed Au to LA ratios. The absorbance spectra were normalized at 300nm. The plasmonic band at 520 nm of Au NPs diminishes at higher LA ratios. 16

Figure 2-2. Normalized absorbance spectra of Au NPs synthesized at 0.38,0.39,0.40 mole ratios of LA to Au. The spectra were normalized at the 300nm to better illustrate the changes in SP band intensity. 18

Figure 2-3. a) UV-Vis spectra feature at representative synthesis steps of the surface plasmon nanoparticle, Au-LA 1-0.39. Absorbance spectra were normalized at 300nm. The emergence of plasmonic band upon reduction was indicated by black arrow. Panel b shows the enlarged view of the pre- reduction curves to better illustrate the trends. Absorbance spectra were normalized at 300nm. The change of absorbance spectra was indicated by the blue arrow. In each panel, final spectrum was highlighted by dash lines. 19

Figure 2-4. Representative absorbance spectra collected under different pHs of Au-LA mixtures prior to reduction. A. different pHs for the same Au:LA mole ratios (1:0.39). B. the same pH (11) of Au:LA mixtures at different mole ratios. The absorbance spectra were normalized at 300nm. 21

Figure 2-5. UV-Vis absorbance spectra of Au-LA 1-0.35 pH adjusted to 12 a) with different times before adding reductant. The green dashed curve showed 0.35 SP NPs in normal synthesized condition as a reference. Absorbance spectra were normalized at 300nm. b) peaks positions and intensities at different times. Noted that at 144 hours the mixture was reduced by 1x reductant resulted in immediately blue-shifted in peaks position to 520nm and increase in peak intensity. 22

Figure 2-6. UV-Vis absorbance spectra of Au-LA 1-0.39 pH adjusted to 12 a) with different times before adding reductant. The green dashed curve showed 0.39 SP NPs in normal synthesized condition as a reference. Absorbance spectra were normalized at 300nm. b) peaks positions and intensities at different times. Noted that at 144 hours the mixture was reduced by 1x reductant resulted in immediately blue-shifted in peaks position to 520nm and increase in peak intensity. 23

Figure 2-7. Reduction of Au:LA 1:0.35mixture by different amount of NaBH4. The absorbance spectra were normalized at 300nm. 24

Figure 2-8. Cyclic Voltammogram of the 1:0.39 Au-LA NPs in a) water and b) organic solvents. Potential scan rate was 0.1V/s. a) Result measured in water with 0.1M $NaClO_4$ as supporting electrolyte after purging with Ar for 20 minutes. b) Result measured in acetonitrile with 0.1M TBAP as supporting electrolyte after purging with Ar for 20 minutes. A 3-electrode system was used including a 0.2 mm platinum disk working electrode, a platinum foil counter electrode, and an Ag/AgCl wire quasi reference electrode. 26

Figure 2-9 Square Wave voltammogram of the 1:0.39 Au-LA plasmonic NPs in a) water and b) organic solvents. Potential scan rate was 0.1V/s. a) Result measured in water with 0.1M

$NaClO_4$ as supporting electrolyte after purging with Ar for 20 minutes. b) Result measured in acetonitrile with 0.1M TBAP as supporting electrolyte after purging with Ar for 20 minutes. The potential values of peaks are listed Result measure in water with 0.1M $NaClO_4$ as supporting electrolyte after purging with Ar for 20 minutes. A 3-electrodes system was used including 0.2 mm platinum disk working electrode, platinum foil counter electrode, and Ag/AgCl reference electrode. Fix accordingly. 26

Figure 2-10. a) Cyclic Voltammogram of the b) Square Wave Voltammogram of 1-0.35 Au-LA NPs in aqueous solvents. Potential scan rate was 0.1V/s. Result measured in water with 0.1M $NaClO_4$ as supporting electrolyte after purging with Ar for 20 minutes. A 3-electrode system was used including a 0.2 mm platinum disk working electrode, a platinum foil counter electrode, and an Ag/AgCl wire quasi reference electrode. 28

Figure 2-11. Differential spectra after electrolysis under different potentials in water with 0.1M $NaClO_4$ supporting electrolyte. Same sample solution split into two was charged to more positive and negative potentials were performed separately to avoid possible irreversible changes to accumulate over stepwise redox charging. The original spectrum which was used as a baseline was subtracted from the spectrum collected after each electrolysis. The arrow pointed out the isosbestic transition at the 520nm plasmonic band. The dash lines indicated key peaks/valleys emerging after the electrolysis under different potentials.... 32

Figure 2-12. comparisons between 1H NMR spectra of free Lipoic acid (bottom panel) and Au-LA 1-0.39 plasmonic Au-LA NCs (top panel) in D2O with the solvent peak at 4.80ppm. 34

Figure 2-13 Comparison between Au-LA NCs a) FT-IR measurements of the non-oxidized and oxidized $Au_{22}LA_{12}$ clusters. Adapted with permission from J. Phys. Chem. C 2014, 118,

20680−20687. Copyright 2014 American Chemical Society, and b) IR spectrum of plasmonic NPs. Spectrum was recorded by the drop-cast sample after air-dried. The broad features around 3000 cm^{-1} are affected by hydrogen bonding from H_2O..... 35

Figure 3-1 Absorbance spectra during the synthesis of the molecular like nanoclusters. Arrow indicates the increase in time/process. 43

Figure 3-2. Absorbance spectra of Au-LA mixture at different time points. Red curve showed the spectrum of the Au-LA right after they were combined. Blue, yellow, green and grey curves are absorbance spectra of the Au-LA mixture after vigorously stirring collected at 1, 2, 3, 4 hours respectively. The black arrow showed the trend of the changing. The spectra absorbance at 300 nm were normalized to one..... 44

Figure 3-3. UV-Vis spectra of Au-LA mixture after reductant addition. Red curve showed the spectrum of the Au-LA right after the addition of 5x reductant. Blue, yellow, green and grey curves are absorbance spectra of the reduced Au-LA mixture vigorously stirring at 1, 2.5, 16, and 20 hours respectively. The black arrow showed the trend of the changing. Thicker line was used to highlight the final curve. 45

Figure 3-4 a) Photoluminescence spectra during reduction. Photoluminescence spectra were normalized by the absorbance at the excitation wavelength of 400 nm. b) corrected/normalized photoluminescence intensity at emission peaks 750nm..... 46

Figure 3-5 Normalized absorbance spectra of nanocluster using different purification methods. The absorbance spectra were normalized at 300nm. 47

Figure 3-6 Normalized luminescence spectra of the same batch NCs using different purification method. Each spectrum was divided by the absorbance at 400 nm from the same solution

to one. In other words, the concentration of different samples were normalized to be the same. 48

Figure 3-7. a) absorbance and b) photoluminescence spectra of NCs synthesized from different Au-LA ratios. The absorbance spectra were normalized at 300nm. The photoluminescence spectra in b were excited at 400 nm and normalized by absorbance value at 400nm. 50

Figure 3-8. a) Normalized Absorbance spectra b) Normalized corrected photoluminescence spectra and c) excitation spectra of molecular like nanoparticles with different reductant (1x, 5x and 10x) ratio compared to a mole of Gold. 1.7X LA:Au. All NCs were purified by dialysis method. The absorbance spectra were normalized at 300nm. The photoluminescence spectra in b were excited at 400 nm and normalized by absorbance value at 400nm. The break on wavelength axis separates the response from two different detectors in luminescence spectra in b. Raw data of excitation spectra were shown in c, the detection was at peak of the emission spectrum for each sample (1x was at 730nm, 5x was at 780nm, and 10 was at 820nm). 52

Figure 3-9 FTIR spectra of a) molecular like NCs by ultra-centrifuge, b) molecular like NCs by dialysis and c) Plasmonic NPs. Each spectrum was recorded by drop-casting the sample and air-dried. The broad features around 3000 cm^{-1} are affected by hydrogen bonding from H_2O. Top panel is FTIR spectra of Lipoic acid for reference. 55

Figure 3-10 1D ^1H NMR spectra of Lipoic Acid compare with Au-LA NPs in D_2O with solvent peak at 4.80ppm. The NCs structure is only one in three possible structures. 56

Figure 3-11 The COSY spectrum of dialyzed Au-LA NCs in D_2O with solvent peak at 4.80ppm. 57

Figure 3-12. Basic representation of Au-LA 1-1.7 nanocluster. Only two different ligand forms are sketched for clarity. 58

Figure 3-13. CV and SWV of the Au-LA Clusters NCs via ultracentrifuge purification? in H2O. The NCs solution was purged with Ar for 15-30 mins with 0.1 M NaClO4 as the supporting electrolyte. A 0.2 mm platinum disk working electrode, platinum foil counter, and an Ag/AgCl wire were used in all measurements. 59

Figure 3-14. Differential spectra of ultra-centrifuged Au-LA 1-1.7 NCs after electrolysis under different potentials. The Au NCs were dissolved in water to have an absorbance at 300 nm around 0.3 with 0.1M $NaClO_4$ supporting electrolyte. The analysis to more positive and negative potentials was performed separately to avoid possible irreversible changes to accumulate over stepwise redox charging. The original spectrum before electrolysis was used as a baseline for subtraction. The vertical dash lines indicate the three absorbance bands in original absorbance spectrum which are 500nm, 590nm, and 680nm respectively from left to right. The changes in absorbance spectra were enlarged in the inset for the bottom panel. 62

Figure 3-15. Raw data of absorbance spectra of electrolysis scans of molecular like Au-1.7 LA NCs 63

Figure 3-16. Normalized photoluminescence spectra of molecular like Au-LA NC annealed with reduced Glutathione at 60 degrees Celsius. Luminescence spectra were normalized by the absorbance at the excitation wavelength of 400 nm. 65

Figure 3-17 Normalized photoluminescence intensity at 800nm at different steps of the annealing process with MonoThiolate reduced Glutathione. 66

Figure 3-18 H NMR spectra of purified annealed sample compare with Au-LA NPs and Glutathione in D_2O with solvent peak at 4.80ppm. 67

Figure 3-19 COSY spectrum of the purified annealed sample in D_2O with solvent peak at 4.80ppm. 68

Figure 3-20 FTIR spectrum of the annealed sample after purification. Spectrum was recorded by the drop-cast sample after air-dried. The broad features around 3000 cm^{-1} are affected by hydrogen bonding from H_2O. 69

Figure 3-21. The NMR spectrum of LA reduced by TCEP and spectra of TCEP and LA as references. All spectra were taken in D_2O with solvent peak at 4.80ppm. Red circles indicated the existence of DHLA and black arrows indicated oxidized TCEP. 70

Figure 3-22. Raw data of a) UV-Vis spectra of NCs before and after the addition of TCEP. b) photoluminescence of the NCs before and after the addition of TCEP. 71

Figure 3-23 Normalized emission spectra of molecular like Au-LA NCs during the annealed process with aqueous DHLA at 60^{o}C. Luminescence spectra were normalized by the absorbance at the excitation wavelength of 400 nm. 72

Figure 3-24 Normalized photoluminescence intensity at 800nm during the annealing process. Note in separate measurements (not shown), the emission intensities decrease significantly after longer annealing time. 73

Figure 3-25. CV-ECL of Au-LA (A) and Au-LA annealed by DHLA (B). Data collected with 25 mM HEPES as ECL co-reactants and 0.2 M $NaClO_4$ as supporting electrolyte. The black line is CV, and the blue line is ECL. Potential range is from -1.2 to 1.2 V. Glassy carbon as working electrode, Pt foil as a counter electrode, and Ag/AgCl as a reference electrode. 74

LIST OF ABBREVIATIONS

Au DTCs	Gold DiThiolate Clusters
Au MPCs	Gold Monolayer-Protected Clusters
Au MTCs	Gold Mixed Thiolate Clusters
Au NCs	Gold nanoclusters
Au NPs	Gold nanoparticles
COSY	Correlated Spectroscopy
CV	Cyclic Voltammetry
DPV	Differential Pulse Voltammetry
FT-IR	Fourier-Transform Infrared Spectroscopy
HOMO	Highest Occupied Molecular Orbital
LA	lipoic acid
LUMO	Lowest Unoccupied Molecular Orbital
MS	mass spectrometry
$NaCLO_4$	Sodium Perchlorate
NCs	nanoclusters
NMR	nuclear magnetic resonance
NPs	nanoparticles
ppm	parts per million
QE	quantum efficiency
SP AuNPs	surface plasmonic gold nanoparticles
SWV	Square Wave Voltammetry
TBAP	Tetrabutylammonium Perchlorate

TEM	Transmission Electron Microscopy
TOABr	Tetraoctylammonium Bromide
UV	ultraviolet
UV-Vis	Ultraviolet-Visible
Vis	visible

1 INTRODUCTION

1.1 Chemistry and Nanomaterials

The nanomaterials field involves the design, analysis, fabrication, and application of structures, devices, and systems by manipulating shapes and sizes on a nanometer scale (nm, 1 nm = 10^{-9} m).[1] Nanomaterials are located between the quantum properties of atoms and the bulk properties of materials. The critical length of properties in bulk materials is minor compared to the size of substances. This is not the case for nanomaterials which results in many interesting features. Material's properties at this tiny scale can be very different because of the relatively larger surface area and quantum effect. At the nanometer scale, a significant number of atoms locate on the surface and affect its properties, making it different with natural scale material. Nanomaterials' properties not only depend on size and shape but also depend on the interface.

Furthermore, the optical, electrical, and magnetic behavior of nanomaterials are influenced by quantum effects. Nanomaterials have fewer atoms and the quantum effects cannot be normalized to ignore the facultative fluctuations. Consequently, quantum effects can dominate the performance of the materials.

Due to the same size scale, nanomaterials are very significant in biological system applications. Many proteins are around 10 nm in size. Nanomaterials can be designed and fabricated at this same scale for modifying and probing biological systems. With specific size, shape, and function, nanomaterials can be used as drug delivery agents, labeling agents, and sensors.[2]

There are two methods to fabricate nanomaterials: bottom-up and top-down. Norio Taniguchi introduced the top-down method in 1974 using larger materials to make nanoparticles.[3] Ten years later, K Eric Drexler proposed the Bottom-Up method to form nanoparticles from atoms.[4]

Under those two methods, there are four ways to fabricate nanomaterials: wet chemical, nanomechanical, thermal evaporation, and gas-phase method. Strengths and weaknesses of each technique can be considered for several materials depending on material requirements and laboratory conditions. Due to our lab interests and conditions, the bottom-up wet chemical method was concentrated to synthesize gold nanoparticles (Au NPs). Wet chemical methods include sol-gel and co-precipitation. According to this method, different ionic solutions are mixed in a suitable proportion, under the influence of temperature, pressure, and pH conditions such that the nanomaterials are precipitated from the solution. After filtration and subsequent drying, nanoscale materials are obtained. The advantages of wet chemical methods are that nanomaterials can be made in a variety of materials, including inorganic, organic and metal materials. Advantages of this method include low costs and the ability to make a large amount of material, however efficiency and the heterogeneous product are sacrificed.

1.2 Three-dimensional spherical Gold Nanomaterials

Nanoparticles (NPs) are an essential material in nanotechnology that have great applications in biological imaging, biosensing, drug delivery, and catalysis. NPs are a combination of 10^6 atoms or fewer bonded together with a size range of 1-100 nm. They are smaller than bulk solid but larger than individual atoms and molecules.[5] As a consequence of NP size, NPs' properties strongly depend on particle size, shapes, interparticle distances, and protecting shell properties,[6] thereby giving rise to three significant features: high surface to volume ratio, quantum size effect, [7] and electrodynamic interactions.[5]

Noble metal nanoparticles are new materials which have stimulated research interests extensively because of their wide range of application due to interesting optical and electronic properties.[8] Noble metal NPs are made from a metal core composed of such metals as copper,

silver, gold, etc. Gold nanoparticles (Au NPs) are the most stable metal nanoparticles, acting as the intermediate and bridge between the chemical properties of bulk gold and atomic gold.[5-6]

Scientific research on Gold NPs did not start until the mid-19th century, even though they were used since ancient times for a decorative purpose. In 1857, Micheal Faraday reduced gold salt with phosphorus in the two-phase system to the created deep-red solution of colloidal gold.[9] This work stimulated intensive interest in research on metal colloids. The earliest examples of NPs were NPs protected by halides and phosphates. However, for the last several decades thiolates have become increasingly important.

NPs can be organic or water soluble depending on the ligand used. This research focused on aqueous thiol ligand stabilized gold nanoparticles, including both nanoclusters (NCs) and surface plasmon nanoparticles (SP NPs) regimes. Nanoclusters are smaller size nanoparticles, with a dimension less than 2 nm and exhibit molecular-like behavior, while SP NPs are larger NPs. Gold nanoclusters (Au NCs) have higher quantum efficiency several times more than bulk gold,[10] while surface plasmon gold nanoparticles (SP Au NPs) have no photoluminescence and are identified by plasmonic bands at 520 nm in absorbance spectra.

Gold monolayer-protected clusters (MPCs) are nanoparticles consisting of a gold core and a self-assembled monolayer (SAMs). The core is composed of multiple gold atoms (ten to hundreds) packed by Au-Au bonding surrounded by a thiol ligand used to stabilize the gold core by strong sulfur-gold bonds. The gold core was stabilized and protected from aggregation to reach bulk gold behaviors. Unique size-dependent capacities are provided by the gold core and the monolayer which protected the core, offering particles robust stabilities. Nanoclusters need to be in ultra-small size (<2 nm) to have quantum confinement effects. Therefore, appropriate strong passivating ligands are necessary to terminate the growing of gold core at early stages.[8]

The monolayer can also be modified to product new surface functionalities. Two common Au NPs synthetic techniques are Brust-Schiffrin synthesis[11-12] and polyamidoamine (PAMAM).[13]

The Brust-Schiffrin method used thiol to stabilize the gold core by a two-phase synthesis process. This method is imperative and has had an outstanding impact in the nanoparticles synthesis field since 1994.[11] For the first time, Au NPs were synthesized thermally and are air-stable with reduced dispersity and controlled size. Briefly, chloroauric acid was transferred to the organic phase with the use of tetraoctylammonium bromide (TOABr), then reduced by organic thiol to form gold-thiolate polymers. At this stage the gold is reduced from Au (III) to Au (I) in the organic phase by thiol. Finally, gold-thiol polymers can be further reduced by aqueous sodium borohydride ($NaBH_4$) to product Au (0).[12] Unfortunately, products of Brust-Shiffrin are often polydisperse.

1.2.1 Plasmonic gold nanoparticles

Surface plasmon gold nanoparticles (SP AuNPs) are relatively large (>2.2nm) and exhibit surface plasmon resonance. Larger spherical gold nanoparticles quickly heat up, resulting in a local area of intense heat when absorbing visible light and are identified by the plasmonic band at about 520 nm in the absorbance spectrum. The deep wine-red color reflects the surface plasmon band (SPB).[6] The color of NPs depends on its size and shape as well as the dielectric constant of the surrounding medium. The plasmonic band's position is size dependent, and intensity is proportional to the core size due to the onset of quantum confinement. Position and width of the bands are also influenced by the shape of the nanoparticles. The absorbance coefficient of plasmonic absorbance is larger than dyes leading to higher detecting sensitivity.[2] The SPR does not exist in Au NCs smaller than 2nm as well as bulk gold.

Gold has a valence electron with a mean free path of 50nm. Thus, there is no light scattering for particles smaller than this. When the wavelength of light is much larger than the particle's size, the free electron will oscillate due to the standing resonance conditions. Under these conditions, electron density will be polarized to one surface and oscillates. When shape and size change on the surface, the electric field density will be shifted, causing the oscillation frequency of the electron to change, affecting optical properties.[2] The plasmonic band disappears at sizes equal to bulk gold. The smallest Au NPs to support plasmon resonance are Au_{329} with 76.3 kDa and about 2.0nm in size.[14-15]

Plasmonic gold nanoparticles drew significant attention in research as a possible target anti-cancer. [16] The SP AuNPs are used in many other applications. The first practical application of NPs was making colorful glasses for over one thousand years by gold nanospheres. Gold colloids have also been used in colorimetric sensing[17] and surface-enhanced Raman scattering[18]. SPB has drawn much attention in the photographic process. It provides information on the development of band structure of metal, aiding the study of optical spectroscopic properties of Au NPs.

1.2.2 Molecular-like gold nanoclusters

Molecular-like gold nanoclusters are very small particles (smaller than 2nm). In this small regime nanoclusters (NCs) show strong quantum confinement of electrons, leading to discrete electronic structure called HOMO-LUMO gap and molecule-like optical properties.[19] The HOMO-LUMO gap is the energy gap between the highest occupied molecular orbital and the lowest unoccupied molecular orbital. The energy relaxation through this gap leads to photoluminescence in the visible near-infrared (NIR) region.[20] Au NPs in the molecular-like range also show a large Stokes shift, which is the difference between excitation and emission

wavelength, predicting significant relaxation energy.[20] Thus, the interaction between the Au core and the sulfur atomic orbital is the key for improving the optical properties of Au NPs. Furthermore, core sizes and ligands can also affect the emission.[21]

One of the essential properties of water-soluble molecular like AuNPs is visible photoluminescence, which is a hypothetical mechanism involving $5d^{10}$ to $6sp^{1}$ interband transition.[22] Photoluminescence is the emission of photons in excited compounds; it is the crucial property of nanoparticles in biological imaging and sensing. Compounds in the ground state absorb energy in the form of photons and are excited into higher energy levels called excited states. These transitions to different excited states result in different bands in spectroscopy. These processes are rapid at around 10^{-15} seconds. After that, compounds follow relaxation processes, emit photons and return to the ground state S_0 level. The two types of photoluminescence which are fluorescence and phosphorescence. Fluorescence is the emitting of photons during relaxation from singlet excited state S_1 to ground state S_0 and have average lifetimes of 10^{-9} seconds. On another hand, phosphorescence takes place from the triplet excited state back to the ground state. Phosphorescence is much slower and has average lifetimes of 10^{-5} to 10^{3} seconds. Interestingly, our gold nanoclusters have lifetimes around 10^{-8} to 10^{-7} seconds, which is too long to be fluorescence and too short to be phosphorescence. Thus, it is a surface emission related somewhere in the middle.

Emission of NPs is less dependent on overall energetics and are more dependent on size and shape than core to ligand interactions (surface state).[20, 23-24] Photoluminescence spectrometry is the method used to record the number of photons emitted during the photoluminescence process and determine the quantum quantity. This quantum quantity is significant in sensing and

imaging purposes. Furthermore, Au NPs have been used in sensing and imaging purposes for their long lifetimes, large Stokes shift, and easy to use in Vivo environmental properties.[25]

There are several characteristic techniques to determine NPs cores dimensions: scanning tunneling microscopy (STM), atomic force microscopy (AFM), small-angle X-ray scattering (SAXS), laser desorption-ionization mass spectrometry (LDI-MS), and X-ray diffraction; along with high-resolution transmission electron microscopy (HRTEM) which is the most common techniques for characterization of NPs, resulting in the photograph of gold cores. TEM photographs show the gold cores' size and distribution, providing crucial information about the dispersity of NPs sample.[26] Otherwise, Ligand of the NPs was identified by UV-Vis, IR, and NMR techniques. In NMR, the atoms close to the core will broaden the signal.[19, 26]

1.3 Roles of stabilizing ligands

Lipoic acid (LA) was used in this work to create water-soluble nanoparticles, which have drawn significant research interest due to the biosystem applications.[27] LA was first identified in 1951 by Lester Reed and his team.[28] It existed in R and S-enantiomer, but only the R form is essential in biological systems and has drawn most of the research interest. LA is a coenzyme in energy metabolism and effects several disease states as well as the tissues.[29] These effects account for the thiol/disulfide exchange reactions which are very important in the nanoparticle's core-ligand interface.

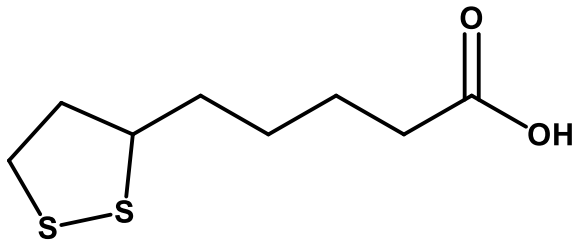

Figure 1-1. Lipoic acid structure.

LA is an organosulfur compound derived from an octanoic acid and considered oxidized because of two sulfur atoms at C6 And C8 connected by a disulfide bond. The five-atom disulfide ring of LA will be open when binding to Au and form 1,3 dithiolate-Au interaction.[30] LA has moderate absorbance band at 333nm due to the hindered dithiolane ring,[31] which will be broken when attaching to the Au core. The redox activities of LA in the thio-disulfide conversions fetch numerous medical and nutritional functions.[27]

LA has been an interest in our group for the synthesize Au NPs because it has two sulfur atoms that provide the multidentate dithiol/thiolate core ligand binding, [32-34] which is entropy favored and theoretically will improve the stability of the monolayer.[35-36] Additionally, the possible thiol-bringing "stable" motif (RS-Au-RS) will affect the optical and electrochemical properties.[32, 34, 37]

In this research, both plasmonic and molecular like Au-LA NPs were synthesized and characterized. Furthermore, the molecular like nanocluster was further enhanced by the annealing method to improve the luminescence QE which is very important in biological applications.

1.4 Motivation

Developing, optimizing, and characterizing new Au NPs extends many potential applications for drug delivery, cell imaging, sensor application or energy application and is the

broad perspective of this research. Characteristic properties such as absorbance, emission, nanocluster charge, size, and ligand play a significant role in proficiency. In our group's previous work, Jia Jang et al. synthesized Lipoic Acid-Gold nanocluster (Au-LA NCs) by a ratio of 1:3 of Au: LA molar ratio. The nanocluster was believed to have the structure of $Au_{22}LA_{12}$. The ultraviolet-visible (UV-Vis) absorbance spectrum of the cluster showed a 505nm band which is the indication of the Au_{22} core size. As mentioned above, LA has two sulfur (S) atoms and some were oxidized and formed SO_x functional groups that affected the optical properties of the cluster. The oxidation process was done during dialysis purification processes which resulted in the enhancement of the cluster photoluminescence QE from 1% to 10%. 10-fold enhancement in photoluminescence and the loss of 505nm band were reported between non-oxidized and oxidized species.[30]

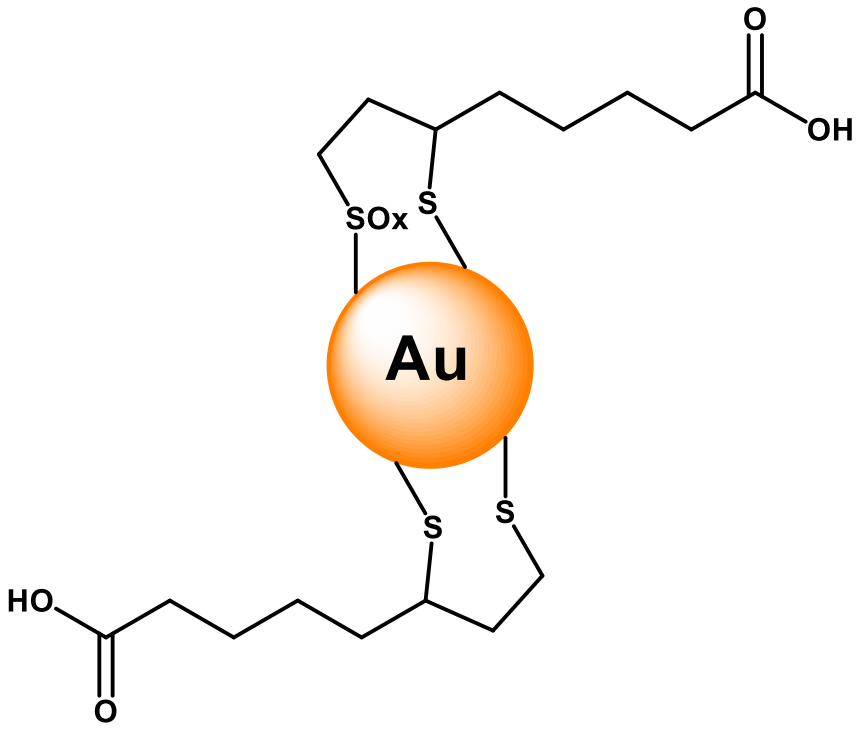

Figure 1-2. Basic representation of $Au_{22}LA_{12}$ nanocluster. Only two different ligand forms are sketched for clarity. The metal NCs are often described by unique compositions with discrete numbers of metal atoms and ligands.

My research was to continue the gold-lipoic acid nanoparticle project by investing in different ratios of gold to lipoic acid, and then optimizing and characterizing them. Furthermore, enhancement of the QE of near IR luminescence was also a focus. To synthesize the Au-LA NPs, LA/$AuCl_4$ mixture was reduced in water by $NaBH_4$. The size of the Au-LA NPs was tuned by varying the ratios of LA to Au. The size difference of the NPs can be demonstrated by absorbance due to size confinement effects. With lower ligand to gold ratio, the surface plasmon NPs are synthesized and are characterized by the absorbance band at 520nm. No photoluminescence was expected for plasmonic NPs.

With a higher ligand to gold ratio, molecular-sized nanoclusters (NCs) were expected because more excess thiol will passivate the gold surface and terminate the agglomeration process. Optical properties are significant for molecular like NCs, therefore many techniques were used to enhance and characterize the smaller NCs. Besides Au-LA ratios, different synthesis conditions also were optimized. After the synthesis process, Au-LA NPs were characterized by conventional analysis techniques such as UV-VIS spectroscopy, photoluminescence spectroscopy, nuclear magnetic resonance spectroscopy (NMR), infrared spectroscopy (IR); however, UV-Vis and photoluminescence were the most exciting technique.

Furthermore, tailoring existing NPs is also a usual research approach to improve the NPs properties to fit potential applications. One of the standard techniques is annealing under the presence of excess thiol. In annealing, moderate excess thiol and a higher temperature is used to optimize the core-ligand interface. However, it is also possible the annealing process results in the elimination of Au NPs with less favorable thermodynamic stability. In my research, the monothiol reduced Glu and dithiol DHLA was used as excess thiol source to anneal the molecular like NPs.

2 EMERGENCE OF SURFACE PLASMON RESONANCE: FROM GOLD NANOCLUSTERS TO NANOPARTICLES WITH MULTIDENTATE LIGANDS LIPOIC ACID

2.1 Abstract

Nanomaterials have drawn intensive research interest due to their size-dependent properties and extensive potentials in various applications. Nano is the dimension in the transition regime from atoms/molecules to bulk. For smaller nanoclusters (NCs) and larger nanoparticles (NPs), the transition point or zone has not been established which has significant implications on the physicochemical properties particularly electrochemical and optical electronic transitions. Using lipoic acid (LA) as multidentate stabilizing ligands, a series of gold nanoparticles were synthesized and characterized among which surface plasmon resonance band varies from indistinguishable to obvious. The size of the Au-LA NPs was tuned by varying the mole ratios of reactants during synthesis. The transition from NCs to NPs with distinct SP band was found at 1:0.39 Au-LA ratio. The synthesis was optimized by manipulating related parameters based on feedbacks from in-situ spectroscopic monitoring. NMR and IR spectroscopy method also performed to characterize the ligand composition as well as the ligand-core interactions. Spectroelectrochemistry and other electrochemistry and optical methods were used to investigate the energy states and electron transfers.

2.2 Background and strategy

One of the most well-known and unique properties of noble metal nanomaterials particularly gold is localized surface plasmon resonance (SPR). The fascinating features of such NPs have drawn intense attention in research.[16] When light irradiates the metallic NPs, electrons in the nanostructure oscillate driven by the electromagnetic field. The light will be absorbed by

the nanostructure at the collective oscillation's resonant frequency, giving rise to a plasmonic band in absorbance spectrum. Work in this chapter focusses on the small spherical gold nanoparticles stabilized by covalently attached multidentate dithiolate ligands, which have weak absorbance plasmonic band at around 520nm with red wine color.[8, 16] For larger nanospheres, the SPR band shifts toward longer wavelength. Nanorod, elongated or irregular/asymmetric nanostructures could have more than one surface plasmon bands in absorbance spectrum. A smaller metal core, or less electron, provides better opportunities to reveal the impact of ligand bonding on the electronic properties of metallic nanomaterials.

When the size of gold nanoparticles gets smaller to approach molecular like nanoclusters regime, the surface plasmon resonance features gradually diminish, and distinct bands emerge in the UV-Vis absorption spectrum.[38] The transition corresponds to the split of the continuum energy states in metal and the distribution of density of states. The transition point between plasmonic NPs and NCs is important for the physical properties of metal nanomaterials and has never been fully characterized. The main motivation of this work is to better understand the unique electrochemical and optical features at this transition point or zone.

The synthesis of nanomaterials of different sizes or shapes have been well-established in literature. For larger nanostructures, lattice structures are often formed which suggest the thermodynamics parameters could dominate the reaction and thus the products. For smaller nanostructures, the synthesis is frequently kinetically controlled. The heterogeneity and reproducibility of the synthesized nanostructures are major concerns for their properties and applications. Post-synthesis treatment and isolation are routinely practiced. Choice of the synthesis conditions, particularly the ratio of ligands to gold during synthesis, will greatly affect the size/composition of NPs herein. As mentioned above for small spherical Au NPs, the 520nm

absorbance band is a characteristic signal to identify the plasmonic NPs, and the plasmonic band intensity depends on the size of the NPs. It is therefore feasible and convenient to optimize the synthesis based on spectroscopic characterizations during the synthetic process. the goal is to identify the NPs from certain core-ligands ratio, reaction time etc. displaying the smallest 520nm bands in UV-Vis spectrum.

Various analytical techniques have been employed to characterize nanomaterials. For inorganic nanomaterials including noble metals, the most used is probably electron microscopes (EM). However, the relatively high energy electrons, in either transmission or scanning EM, could damage the integrity of the nanostructures particularly those small ones such as nanoclusters. Further, organic ligands are invisible in EM analysis which might be less a concern in larger nanomaterials serving as stabilizing agents but plays more significant roles in smaller nanostructures. Regardless, the general understanding of gold nanoparticles established in literature provides foundation for this project. Ligand composition and core-monolayer interaction were investigated by NMR and IR techniques. Cyclic voltammetry and differential pulse voltammetry were used to investigate basic electrochemical properties of the NPs. Spectroelectrochemistry measurements were performed to resolve the changes in absorbance spectra induced by oxidation or reduction of the Au NPs.

2.3 Experimental details

Previous reported synthesis procedure of gold lipoic acid nanoclusters was followed with some modification to synthesize SP NPs.[39] First, a stock gold salt aqueous solution, Hydrogen tetrachloroaurate (III) ($HAuCl_4$:$3H_2O$), was prepared at the concentration of 6.35mM. As expected, the gold(III) solution have a yellow color. Second, a stock lipoic acid solution was

prepared by dissolving 15.75mg of lipoic acid (LA) in 12mL of nano purified water. 1mL of 0.5M sodium hydroxide (NaOH) was added to the lipoic acid stock solution to fully dissolve lipoic acid and form a colorless solution. Next, an allocate of the $HAuCl_4$ solution was mixed with LA stock solution at the designed volume/ratio. Larger ligand: Au ratio will result in the disappearance of the 520nm plasmonic band in absorbance spectrum. The mixture had orange-red color with acidic pH. In the second step, after 5 minutes of vigorously stirring, the pH of the solution was adjusted to 11 by NaOH. The color quickly changed from orange-red to clear yellow after pH changed. In the third step, The Au-LA pH 11 solution was stirred for four hours till the solution became colorless or the absorbance stopped changing. In step four, the Au-LA mixture were reduced by $NaBH_4$ at the designated mole ratio. The solution immediately turned dark brown red. Finally, the solution was purified via ultra-centrifuge.

Four aspects of the synthesis conditions were optimized at each synthetic step as part of this study: a) ratio of LA to Au, b) pH of mixtures at step 2; c) stirring time of the mixture in step 3 and d) the mole ratio of reductant $NaBH_4$ to Au.

2.4 Results and Discussion

2.4.1 Changes in Plasmonic band intensity with the amount of lipoic acid in synthesis.

Because surface plasmon resonance has a convenient optical signature, a band at around 520nm, in visible spectrum range, UV-Vis absorption spectroscopy is the most essential techniques to monitor the syntheses and characterize the products. Figures 2-1 shows the absorbance spectra of Au-LA NPs with the increase in mole ratio of Au: LA during synthesis.

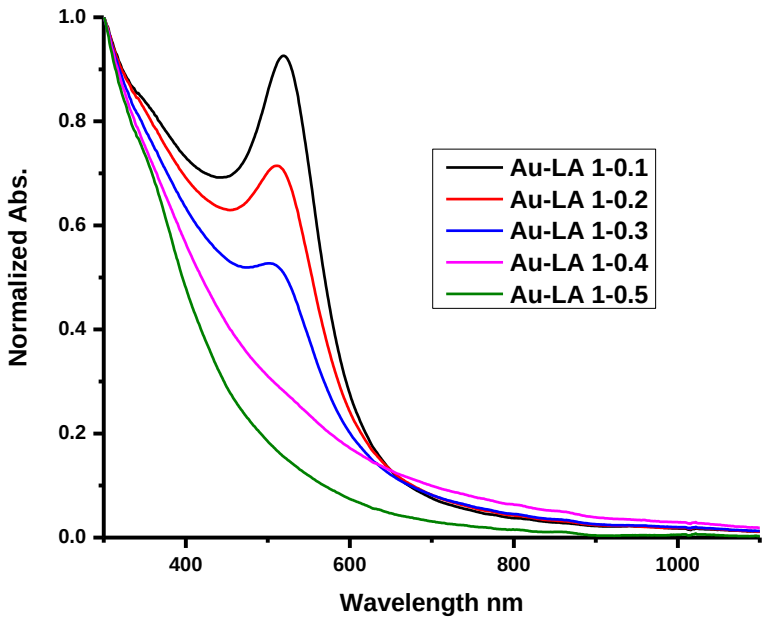

Figure 2-1. Normalized absorbance spectra of different (reaction mixtures/products?) at the listed Au to LA ratios. The absorbance spectra were normalized at 300nm. The plasmonic band at 520 nm of Au NPs diminishes at higher LA ratios.

The formation of the ligand stabilized Au nanoparticles involves simultaneous agglomeration of Au atoms for core growth and thiolate bonding on surface which stops further growth. Different amount of LA, more specifically different mole ratio to Au, will result in nanoparticles with different average sizes. The products are generally a mixture containing predominantly either thermodynamically stable or kinetically trapped sizes/compositions, or both. A lower ratio of LA will produce redder solutions with more intense 520nm plasmonic bands in absorbance spectra. It is well-known that the higher intensity of the plasmonic band indicates larger sizes of Au NPs. At Au:LA 1:0.1 (note each LA contains two sulfurs for Au bonding unlike mostly used monothiols), a rather intense SP band is observed. With the increase in the LA ratios, the SP band intensity decreases and ultimately disappears at 1:0.4, clearly shown in the normalized overlaid spectra. Concurrent with the disappearance of SP band, the

nanoparticles began to show very weak photoluminescence which was absent at low LA ratios. The near IR photoluminescence is a well-known property of molecular nanoclusters.[19, 30, 40-43] It is also reported that the HOMO-LUMO energy band gap emerges at around 2.2 nm.[8, 19] Therefore, at the ratio of 0.4 with dithiolate ligands, the nanoparticles believed to reach the molecular size or with molecular energetics. The color of the solution of 0.4 LA ratio had a dark brown color which also matches other molecular like Au-LA NCs. The color of the NPs solution provides further support to indicate the transition to molecular like nanoclusters from plasmonic nanoparticles.

After the general transition range from NPs to NCs was identified. Fine Au: LA ratios were deliberately investigated and showed in figure 2-2. The goal is to identify the smallest NPs with discernable SP features, in which impacts by the ligand bonding specifically dithiolates adopted in our group can be better resolved. The UV-Vis spectrum of the 1: 0.39 Au: LA sample (red curve) shows a barely seen tiny hump at 520nm. This NP sample is identified to closely represent the transition and is the focus on further study.

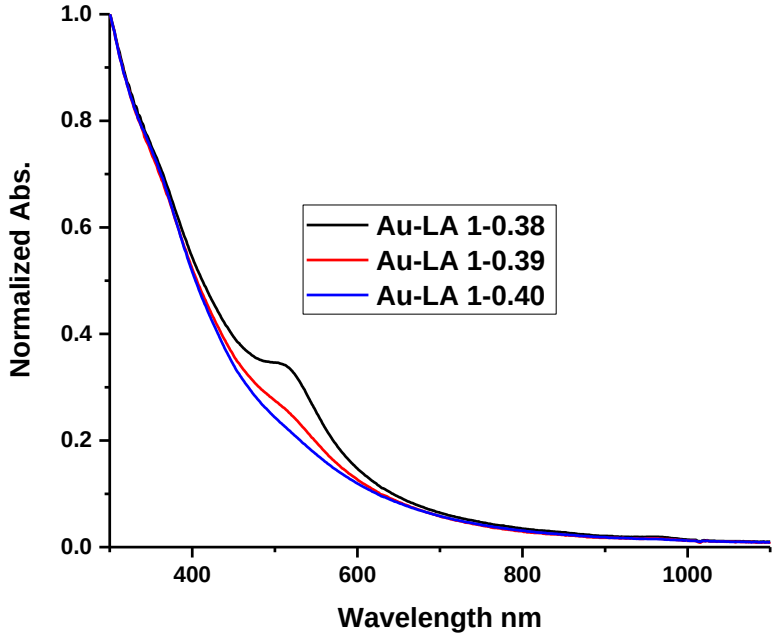

Figure 2-2. Normalized absorbance spectra of Au NPs synthesized at 0.38,0.39,0.40 mole ratios of LA to Au. The spectra were normalized at the 300nm to better illustrate the changes in SP band intensity.

2.4.2 Optimization of synthesis based on spectroscopy monitoring

Spectroscopic features during the synthesis process can provide important feedbacks at each synthetic step for optimization. Unlike nanoclusters, plasmonic NPs have no photoluminescence. Therefore, UV-Vis spectroscopy is the method of choice for its convenience, albeit less sensitive. Figure 2-3 showed the overlaid absorbance spectra of the 1:0.39 Au-LA mixture at representative synthetic steps, from pH adjustment to reductant addition.

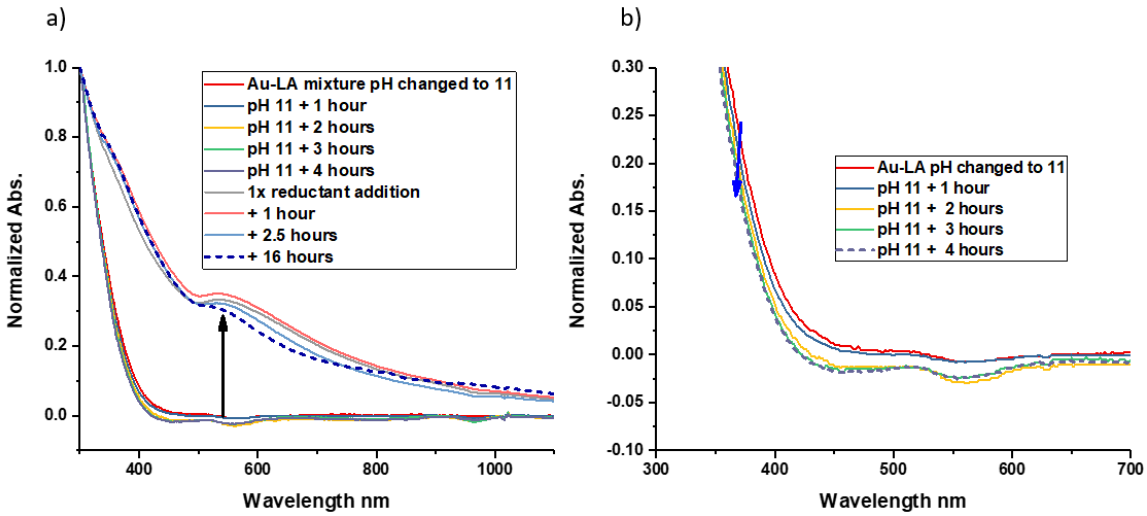

Figure 2-3. a) UV-Vis spectra feature at representative synthesis steps of the surface plasmon nanoparticle, Au-LA 1-0.39. Absorbance spectra were normalized at 300nm. The emergence of plasmonic band upon reduction was indicated by black arrow. Panel b shows the enlarged view of the pre- reduction curves to better illustrate the trends. Absorbance spectra were normalized at 300nm. The change of absorbance spectra was indicated by the blue arrow. In each panel, final spectrum was highlighted by dash lines.

The absorbance spectra throughout the synthesis process showed the development of the 520nm plasmonic band. Indicated by the black arrow, the plasmonic band in absorbance spectrum was only formed after the addition of the reductant along with the immediate change of solution color. Prior to reduction, the sharp decay in absorbance toward longer wavelength is characteristic for Au(I) thiolate complexes. Subtle changes in the absorbance spectra of the Au-LA mixture upon pH adjustment are enlarged in panel B.

It is worth mentioning that the absorbance band of lipoic acid at 330nm[30] disappeared after the addition of $HAuCl_4$. This was due to the five-atom disulfide ring of LA being disrupted upon complexing with Au. Adjustment to basic pH was necessary to improve the solubility of the reaction intermediates, which resulted in more transparent solution. The slight negative absorbance and curvatures were probably due to the normalization at 300 nm when the scattering

by the large polymeric complexes could not be ignored and changed over time. During the incubation after pH adjustment, the mixtures only changed to clear light yellow color instead of colorless solution which was reported in the NCs synthesis process adopting higher ratio of LA.[30]

The 520nm plasmonic band appears quickly after the addition of reductant along with the immediate color change of the mixture from yellow to dark brown-red. The color change and plasmonic band in absorbance spectra indicated the creation of plasmonic Au nanoparticles. The reaction was quenched (by solvent removal?) after 16-hour reduction after the spectrum features stopped changing. Representative spectra are selected to illustrate the dynamic changes during the nanoparticle formation processes. Generally speaking, the band is gradually increasing after 1 hour of the addition of reductant (started from red curve to blue curve) followed by the decrease over time. Importantly, the SP band gets narrower toward the end, suggesting more uniform species being created. As mentioned previously, the Au core growth and ligand surface passivation compete each other and could form poly-dispersed NPs. However, only specific sizes/compositions are thermodynamically stable or can be kinetically isolated. The SP band narrowing along with the decrease in absorption/scattering in the longer wavelength range corresponds to the conversion of less stable species into thermodynamically and/or kinetically favored ones, strongly suggesting the synthesis of a small yet uniform plasmonic AuNPs. It is also interesting to notice a weak broad band within 300-400 nm range appeared upon reduction. The feature is reminiscent of that from the 5-atom ring LA itself, which has been broken prior to reduction. It is attributed to the bonding of both sulfur to Au core which impose similar structure constraint, and confirming the multidentate ligand design. As expected there was no photoluminescence observed during the synthesis process.

2.4.2.1 Impact of pH on the synthesis.

Optimization of synthesis conditions is critical to obtain NPs with desired properties. With the formation of the plasmonic band in absorbance spectra recorded during the synthesis process, the pH of Au-LA mixtures at step 2 (prior to the reduction) was varied. The goal is to understand the pH effect on the formation of more uniform small plasmonic NPs. Absorbance spectra of such analysis are shown in figure 2-4.

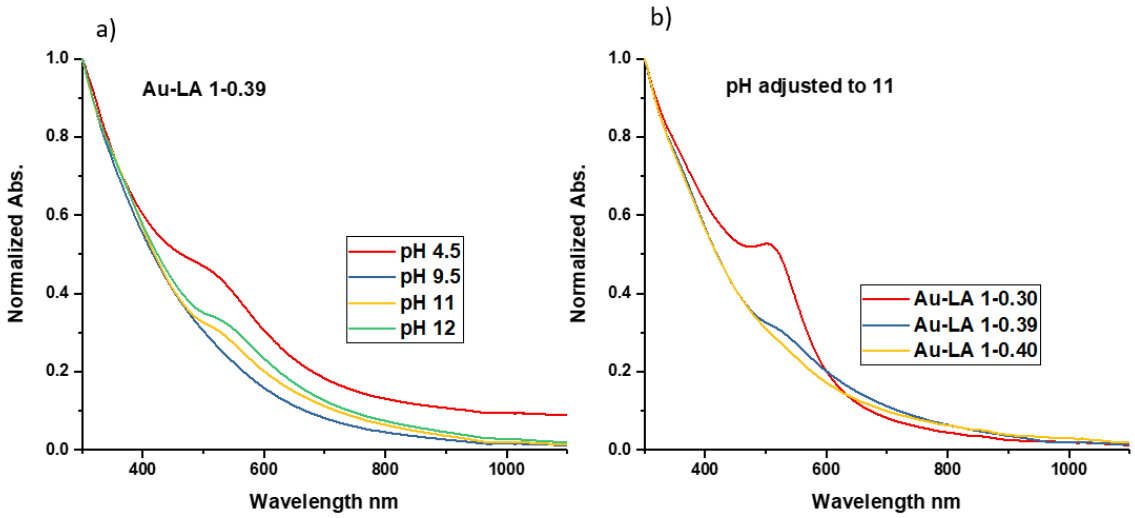

Figure 2-4. Representative absorbance spectra collected under different pHs of Au-LA mixtures prior to reduction. A. different pHs for the same Au:LA mole ratios (1:0.39). B. the same pH (11) of Au:LA mixtures at different mole ratios. The absorbance spectra were normalized at 300nm.

For the same gold to LA ratio mixture, if pH was more acidic for example around pH 4-5, the solution is cloudier which matches the higher tail after plasmonic band 520nm in absorbance. The high background extinction across wavelength is characteristic of scattering by large suspended particles. There was no plasmonic band in absorbance spectra if the pH was within 7 (not shown) to 9.5 range. In other words, there were no plasmonic NPs formed. Only when the

pH was above 11 in step 2, a weak yet defined plasmonic band with low-intensity tail was formed.

As shown in figure 2-4, when the pH of the Au-LA mixture was adjusted to around pH 12, the 520nm plasmonic band also formed over time. The synthesis process under this condition of 1-0.35 and 1-0.39 Au-LA SP NPs was monitored shown in figure 2-5 and 2-6. Formation of Au nanoclusters without reductant addition has been reported via heating/aggregation mechanism.[44] The extra NaOH seemed to induce the formation of plasmonic NPs following similar mechanism that requires further study.

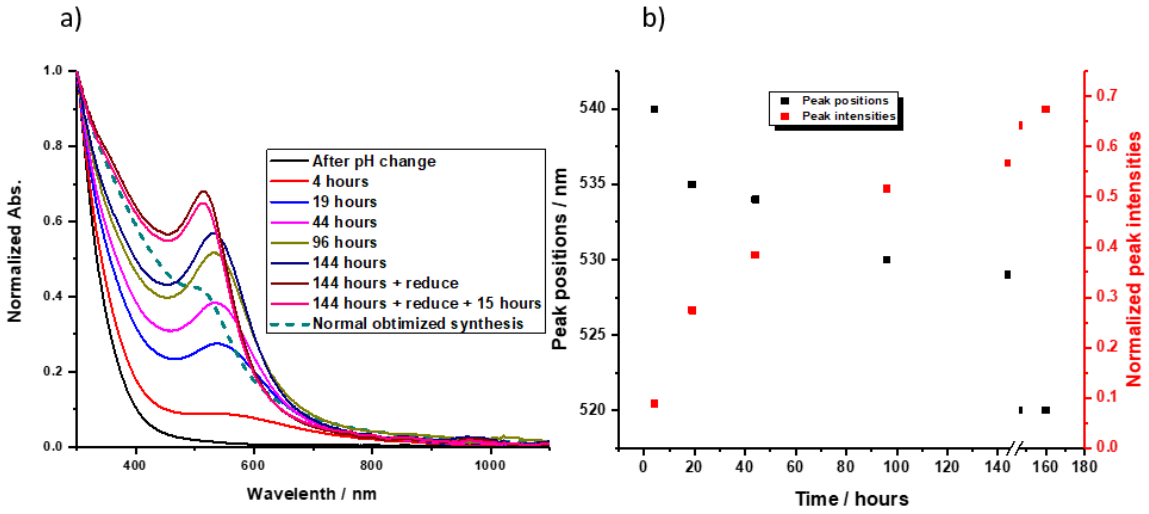

Figure 2-5. UV-Vis absorbance spectra of Au-LA 1-0.35 pH adjusted to 12 a) with different times before adding reductant. The green dashed curve showed 0.35 SP NPs in normal synthesized condition as a reference. Absorbance spectra were normalized at 300nm. b) peaks positions and intensities at different times. Noted that at 144 hours the mixture was reduced by 1x reductant resulted in immediately blue-shifted in peaks position to 520nm and increase in peak intensity.

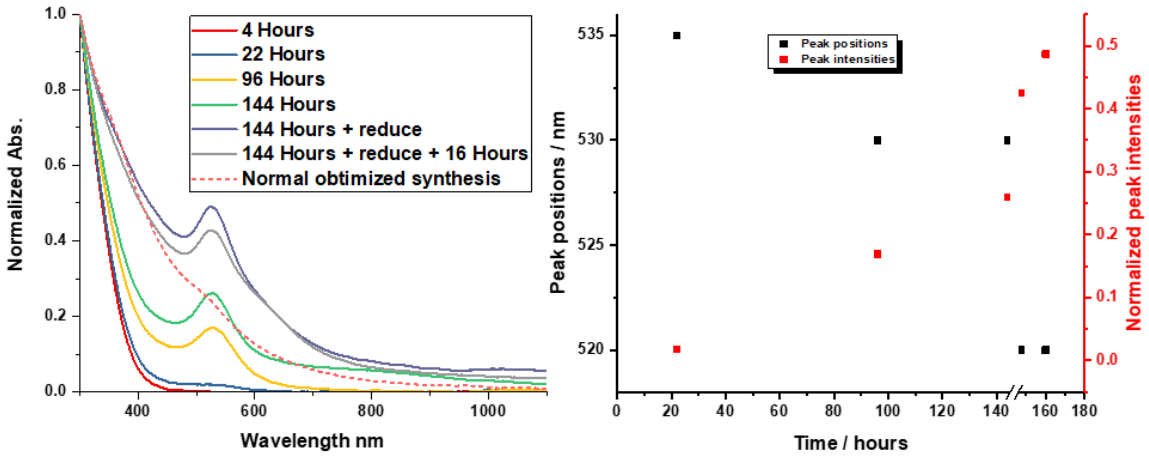

Figure 2-6. UV-Vis absorbance spectra of Au-LA 1-0.39 pH adjusted to 12 a) with different times before adding reductant. The green dashed curve showed 0.39 SP NPs in normal synthesized condition as a reference. Absorbance spectra were normalized at 300nm. b) peaks positions and intensities at different times. Noted that at 144 hours the mixture was reduced by 1x reductant resulted in immediately blue-shifted in peaks position to 520nm and increase in peak intensity.

The stirring time from the point of pH adjustment to the reductant addition also affects the formation of plasmonic NPs. The trend was analyzed in Figure 2-5 and 2-6 panel b. Longer waiting time will result in stronger SP band intensity, or larger NPs. The tailings toward longer wavelength after plasmonic band are relatively low in this series, suggesting high monodispersity. The SP band is red-shifted compared to the reference spectrum which was from an optimized synthesis. As presented the last two absorbance spectra, right after the reductant addition at 144 hours, the SP band immediately shifted back to 520nm. Again, the results indicate the NPs formed without and with reduction are different, though both displaying SP bands, and require further characterizations.

2.4.2.2 Impacts of reduction conditions

The final step in the Brust-Schiffrin synthesis of thiolate stabilized Au nanoparticles is the reduction with NaBH4. Figure 2-7 shows the SP NPs synthesized with different amount of

reductant $NaBH_4$. Given the disulfide LA and basic conditions were sufficient to induce the formation of Au core or Au (0), a relatively lower amount of NaBH4 compared to literature was adopted. Higher amount of the reductant (5x) as shown in blue curve, resulted in higher plasmonic band intensity. The plasmonic band was not shifted and there was minimal baseline scattering confirming a slightly larger size formed at higher amount of reductants.

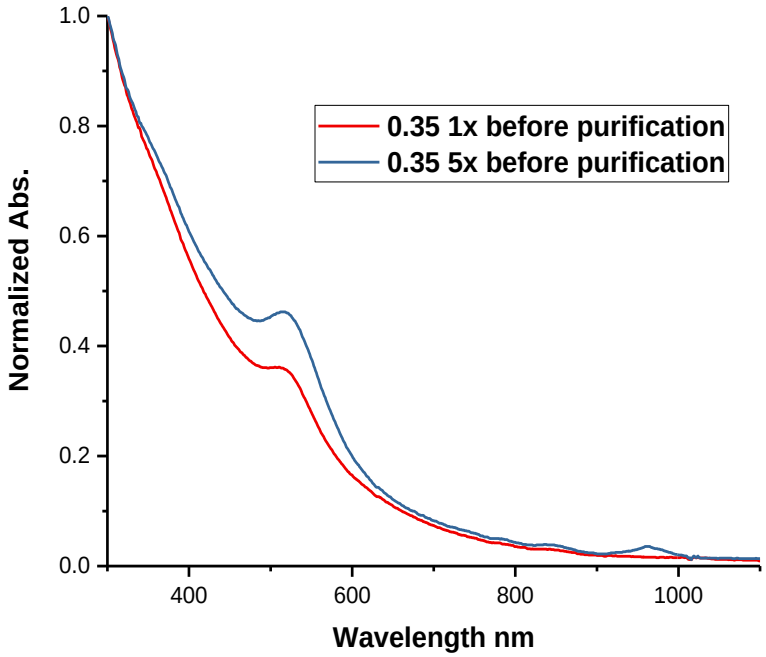

Figure 2-7. Reduction of Au:LA 1:0.35mixture by different amount of NaBH4. The absorbance spectra were normalized at 300nm.

2.4.3 Electrochemical and optical properties of characteristic plasmonic gold nanoparticles

2.4.3.1 Electrochemical characterizations.

We are primarily interested in the properties of the AuNPs in aqueous environment for potential applications. Because water splitting will generate significant background current that

interferes with the signals from target analyte, the potential window was limited to -1 V to 1.2 V in all electrochemical methods. The sample synthesized with 0.39 mole of LA to Au is selected for systematic analysis because it has the weakest SP band, which would likely display the most obvious changes, i.e. signal of interest, upon controlled electron transfer reactions. The tiny plasmonic band, electron oscillation under electromagnetic fields, might be a critical point to reveal the transition of unique electrical properties of noble metal nanomaterials. Figure 2-8 and 2-9 showed the cyclic and square wave voltammograms of the 1:0.39 Au-LA NPs. The redox activities of the same NPs in organic solvent are also collected after phase transfer following our previous report. The goal is to resolve features interfered by water splitting or oxygen reduction.

Because the sample could still contain more than one composition/size, it is essential to employ multiple techniques to identify the main redox activities from the main species. The starting point would be to reference to thiolate stabilized Au nanoclusters, in which the larger ones are smaller than but close to this plasmonic NPs. A well-known feature is quantized double layer (QDL) charging, i.e. multiple uniform peaks (same current amplitudes with comparable potential spacings) corresponds to consecutive one electron transfer activities. Although QDL features have not been observed in plasmonic NPs, and the high dielectric constant of water hampers to detect QDL behavior, the same rationale can be adopted. We attribute the main peaks in CV to the main species of the sample and analyze the corresponding features in pulse voltammetry (SWV) which is more sensitive but complicated with the presence of additional features from minor species.

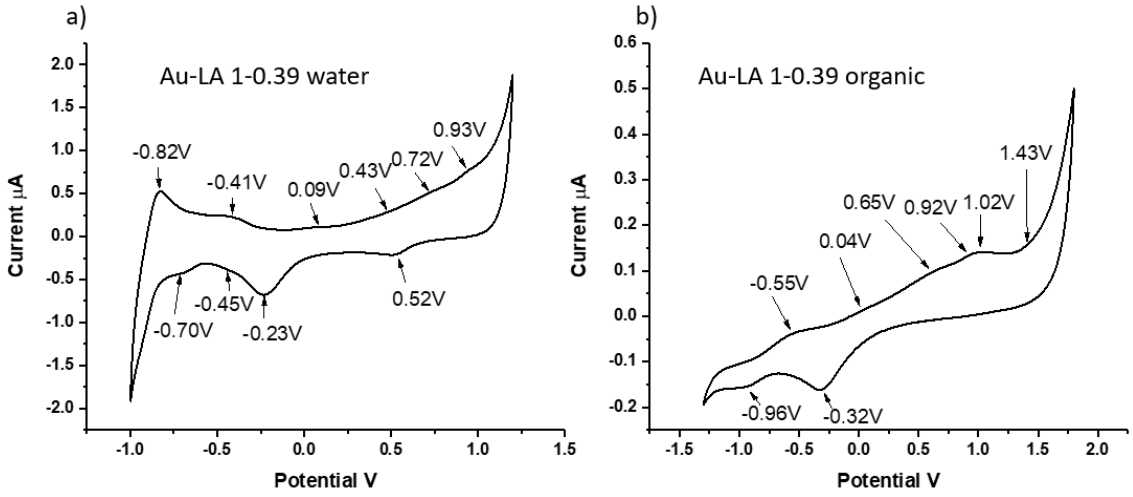

Figure 2-8. Cyclic Voltammogram of the 1:0.39 Au-LA NPs in a) water and b) organic solvents. Potential scan rate was 0.1V/s. a) Result measured in water with 0.1M $NaClO_4$ as supporting electrolyte after purging with Ar for 20 minutes. b) Result measured in acetonitrile with 0.1M TBAP as supporting electrolyte after purging with Ar for 20 minutes. A 3-electrode system was used including a 0.2 mm platinum disk working electrode, a platinum foil counter electrode, and an Ag/AgCl wire quasi reference electrode.

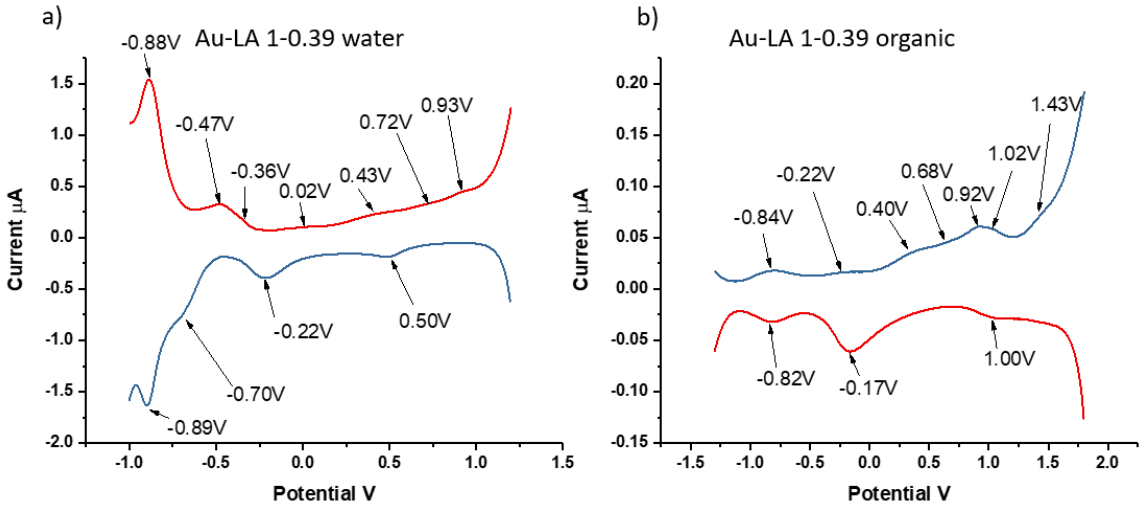

Figure 2-9 Square Wave voltammogram of the 1:0.39 Au-LA plasmonic NPs in a) water and b) organic solvents. Potential scan rate was 0.1V/s. a) Result measured in water with 0.1M $NaClO_4$ as supporting electrolyte after purging with Ar for 20 minutes. b) Result measured in acetonitrile with 0.1M TBAP as supporting electrolyte after purging with Ar for 20 minutes. The potential values of peaks are listed Result measure in water with 0.1M $NaClO_4$ as supporting electrolyte after purging with Ar for 20 minutes. A 3-electrodes system was used including 0.2 mm platinum disk working electrode, platinum foil counter electrode, and Ag/AgCl reference electrode. Fix accordingly.

The main noticeable features in CV include oxidation peaks at -0.41V, 0.09V, 0.43V, 0.72V, 0.93V, and reduction peaks at -0.70V, -0.45V, and 0.52Vas listed in Table 1. The broad cathodic peak around -0.23V with significantly higher current can include the residual oxygen that is practically difficult to remove completely without a glovebox. However, oxygen reduction in organic solvent on Pt electrode appears at around -1.0V vs. a quasi-reference Ag+/Ag electrode. Therefore, the cathodic peak at around -0.3V strongly suggests the -0.23V peak in aqueous measurements results from the AuNCs. Apparently, oxidation toward more positive potentials in both aqueous and organic solvents is not reversible (lack of corresponding reversal reduction peaks in the reversal scan). The two obvious reduction peaks at +0.52 and -0.23V can be explained by the relaxation of electrons at higher energy states. Similar relaxation after oxidation has been observed in large nanoclusters.[45] The plasmonic NPs contain more electrons and thus display similar phenomena. The pulse voltammetry (SWV) analysis confirms those features especially in the oxidation scan. Although the very weak peak current indicates polydispersed sizes, which is common for these types of nanomaterials, the pattern suggests uniform species exist and can be isolated upon further separation or treatments. Specifically, the relative uniform current amplitude for the oxidation peaks strongly suggest the same number of electron transfers at each peak (In convention wisdom, one electron). The peak spacings between adjacent redox activities were also calculated in table 2-1. In oxidation scan SWV, the spacing between peaks were 0.41, 0.11, 0.37 0.4 0.3 and 0.2. Similarly, In the reduction scan SWV's the spacing were 0.18, 0.08, 0.42, 0.68, 0.64. The peak spacing is the key information to investigate the energy diagram and transition state of the NPs and should be focused more in future experiments.

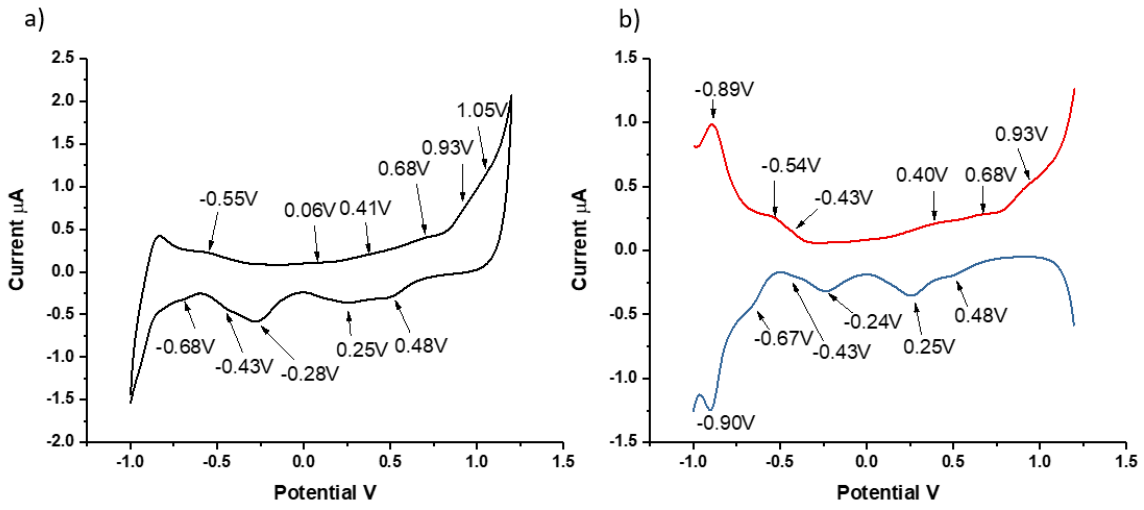

Figure 2-10. a) Cyclic Voltammogram of the b) Square Wave Voltammogram of 1-0.35 Au-LA NPs in aqueous solvents. Potential scan rate was 0.1V/s. Result measured in water with 0.1M $NaClO_4$ as supporting electrolyte after purging with Ar for 20 minutes. A 3-electrode system was used including a 0.2 mm platinum disk working electrode, a platinum foil counter electrode, and an Ag/AgCl wire quasi reference electrode.

For comparison, the redox properties of the 1:0.35 NPs with slightly stronger SP band are plotted in Figure 2-10. The overall features are almost identical between 1-0.35 and 1-0.39 samples. Again, the results suggest the slight variation in the synthetic conditions produced similar products. Albeit the SP band intensity are slightly different, which could be understood by differences in the density of states or free electrons, the energy states are similar.

Table 2-1. Peaks and peak spacings in the oxidation and reduction scans of SWV and CV of Au-LA 1-0.39 in aqueous and organic; And 1-0.35 in aqueous. Red, Blue, and green colors represent the matching signals from the same potential or energy state.

0.39 in H2O									
SWV									
oxidation scan's peaks (V)	-0.88	-0.47	-0.36	0.02	0.43	0.72	0.93		
gap		0.41	0.11	0.38	0.41	0.29	0.21		
reduction scan's peaks (V)	-0.89	-0.70		-0.22	0.50				
gap		0.19		-0.22	0.72				
CV									
oxidation peaks (V)	-0.82	-0.41	-0.41	0.09	0.43	0.72	0.93		
gap		0.41	0.00	0.50	0.34	0.29	0.21		
Reduction peaks (V)		-0.70	-0.45	-0.23	0.52				
gap			0.25	0.22	0.75				
0.39 in ACN 0.1M TBAP									
SWV									
oxidation scan's peaks (V)	-0.84		-0.22		0.40	0.68	0.92	1.02	1.43
gap			0.62		0.62	0.28	0.24	0.10	0.41
reduction scan's peaks (V)	-0.82		-0.17					1.00	
gap			0.65					1.17	
CV									
oxidation peaks (V)		-0.55		0.04		0.65	0.92	1.02	1.43
gap				0.59		0.65	0.27	0.10	0.41
Reduction peaks (V)	-0.96		-0.32						
gap			0.64						
0.35 in H2O									
SWV									
oxidation scan's peaks (V)	-0.89	-0.54	-0.43		0.40	0.68	0.93		
gap		0.35	0.11		0.83	0.28	0.25		
reduction scan's peaks (V)	-0.90	-0.67	-0.43	-0.24	0.25	0.48			
gap		0.23	0.24	0.19	0.49	0.23			
CV									
oxidation peaks (V)		-0.55		0.06	0.41	0.68	0.93	1.05	
gap		-0.55		0.06	0.35	0.27	0.25	0.12	
Reduction peaks (V)		-0.68	-0.43	-0.28	0.25	0.48			
gap			0.25	0.15	0.53	0.23			

2.4.3.2 Spectroelectrochemical analysis of plasmonic NPs.

An ultimate goal to synthesize small plasmonic NPs is to understand the impact of one/few electron oxidation/reduction on the plasmonic behavior. The light-electron interactions in matter is a fundamental question with broad implications on various applications. Electrolysis technique was used to charge the samples to different charge states, i.e. the valley potentials after the corresponding peaks in voltammogram. The electrolysis was performed in a thin

spectroscopic cuvette inside a UV-Vis spectrometer. A Pt mesh working electrode was positioned in the light path. When the light beam passes through the mesh and interacts with the samples near the electrode (within the diffuse layer), the optical changes by electrolysis can be directly recorded. Figure 2-11 showed the spectroelectrochemical analysis of the Au:LA 1-0.39NPs. Interestingly, oxidation (top half of Figure 2.11) and reduction (bottom half) spectra display similar trends. The positive and negative changes indicate the additional and suppressed absorption transitions respectively. Adding an electron by electrolysis into an energy state will suppress the transition to this energy state, while the transition of this extra electron to higher energy state/s will generate new absorption band/s. Creating a hole will induce opposite effects accordingly. If one or both energy states involved in the optical transitions were shifted upon oxidation or reduction, the absorption band/valley would shift accordingly. The top axis of figure 2.11 showed Energy in eV unit corresponding to the wavelength in the bottom axis. The fine spectrum details revealed by charging will allow us to resolve the corresponding energy states more accurately.

The absorbance around the original plasmonic band at 520nm increased upon both oxidation and reduction. In the differential spectra in Figure 2-11, a positive broad band with the peak at around 600-628nm appears after both oxidation and reduction electrolysis of the 0.39 SP NPs. This positive peak remained at 600 nm from all negative potentials up to +0.2V, and then shifted to longer wavelength range at 628 at +1/1.2 V. The features are qualitatively consistent with the voltammetric results. Because of the large amount of free electrons which support the plasmonic behavior, additional electrons by reduction are not anticipated to shift the frontier energy states (i.e. ‘Fermi level’) much. Upon the oxidation at higher positive potentials, reversal

reduction occurred at more negative potentials, +0.52/-0.23V. We postulate the relaxation of electrons at higher energy states and possible structure changes might have contributed.

There are fine differences after oxidation and reduction in the lower 500nm region. Again, the +0.2V data seems to be a separating point/range. The oxidation panel seemed to dispaly the isosbestic point at the plasmonic band 520nm which requires additional measurements. After more positive 1V and 1.2V electrolysis, a sharp peak at 325nm and valley at 379-390nm can be seen. The valley shifted from 379nm to 390 from 1v to 1.2V. The 325nm was not shifted, but there was a twofold increment in the change of absorbance intensity. From 200mV to negative potential, this peak and valley disappeared. There is no significant change from negative potential to 200mV potential electrolysis. The 510nm valley seems to stay the same throughout all potential applied. The shift in SP and differential peaks are significant and provides the experimental evidences for future theoretical analysis

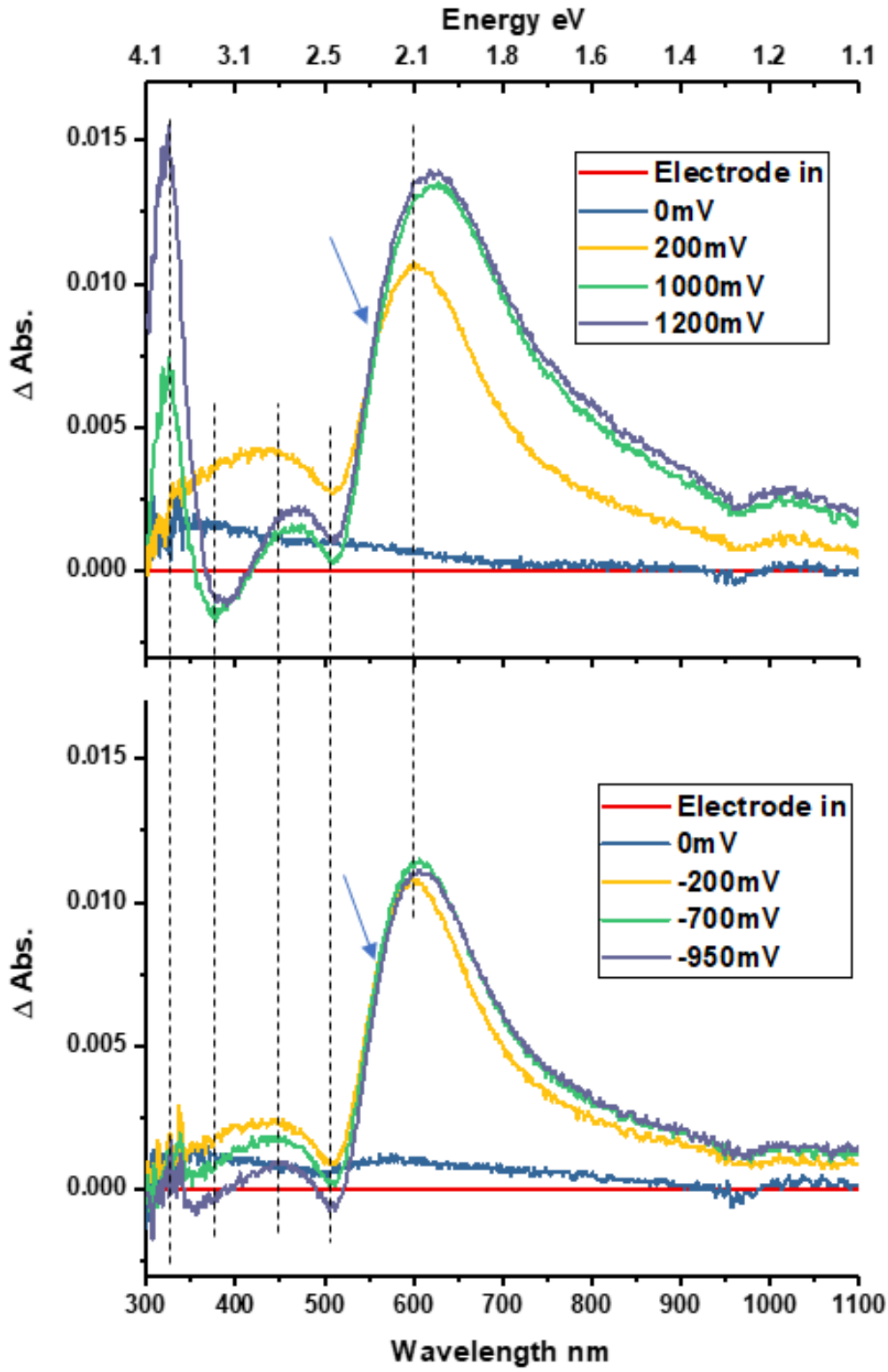

Figure 2-11. Differential spectra after electrolysis under different potentials in water with 0.1M $NaClO_4$ supporting electrolyte. Same sample solution split into two was charged to more positive and negative potentials were performed separately to avoid possible irreversible

changes to accumulate over stepwise redox charging. The original spectrum which was used as a baseline was subtracted from the spectrum collected after each electrolysis. The arrow pointed out the isosbestic transition at the 520nm plasmonic band. The dash lines indicated key peaks/valleys emerging after the electrolysis under different potentials.

Table 2-2. peaks (black color) and valley (red color) position in 0.39 SP NPs Spectro electrochemistry panels.

Positive scans (mV)	Peak 1 (nm)	Valley1 (nm)	Peak 2 (nm)	Valley (nm)	Peak 3 (nm)
200	N/A	N/A	438	510	600
1000	325	379	475	510	628
1200	325	390	475	510	628
Negative scans (mV)					
-200	N/A	N/A	440	510	600
-700	N/A	N/A	440	510	607
-950	N/A	N/A	455	510	607

.

2.4.3.3 Ligand monolayer characterization by Nuclear Magnetic Resonance.

The ^{1}H NMR spectrum of the plasmonic Au NPs is shown in figure 2-12. For reference the disulfide lipoic acid NMR spectrum is also included. The ^{1}H NMR spectrum features of the plasmonic NPs are significantly broader than the ligand itself, similar to the large NCs due to line broadening effect. The line broadening effect results from the heterogeneity in the chemical environment of each type of hydrogen species. Unlike free ligand molecules, those hydrogen atoms closer to the core experience more restricted environment. Because the core is generally not ideally spherical, the corresponding 1H peaks will be broader and shifted depending on the local interactions. Differences in core sizes are another factor that will cause significant broadening of the NMR peaks.

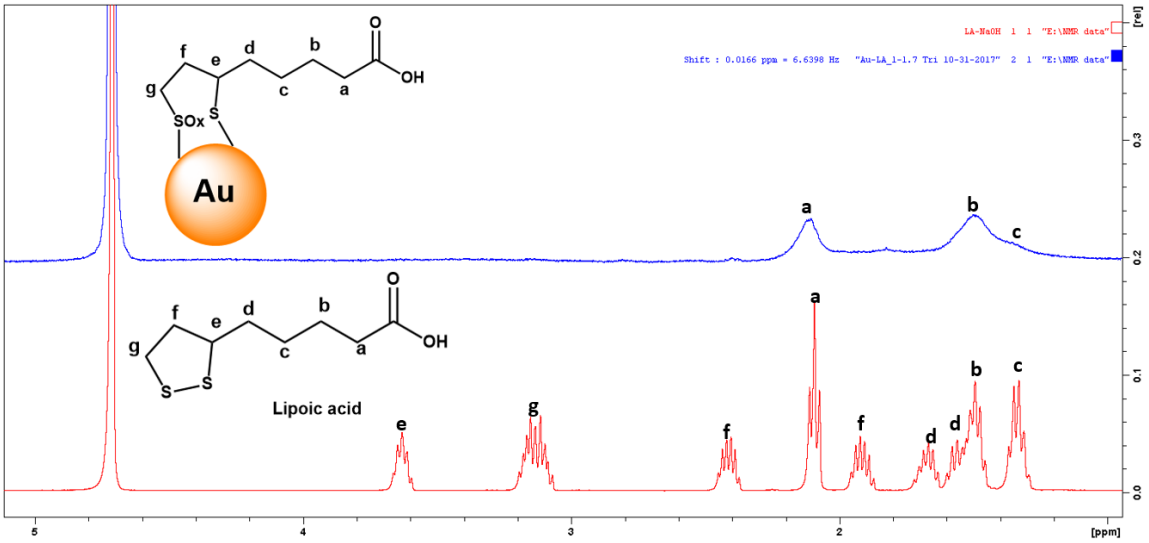

Figure 2-12. comparisons between 1H NMR spectra of free Lipoic acid (bottom panel) and Au-LA 1-0.39 plasmonic Au-LA NCs (top panel) in D2O with the solvent peak at 4.80ppm.

The hydrogen at e, g, f, and d are closer to the core. Considering the surface curvature and the Au core is often not ideally spherical, higher heterogeneity in their chemical environment makes their signals too broad to resolve. The H-b and H-a positions are further away from the core and has sharper peaks which can be resolved from the baseline. The H-c peak is in the middle and displays a little bump on the high field side of H-b signal. Even though the NMR spectrum could not resolve all hydrogen signals from the ligands, the results clearly indicate the successful purification of unbound lipoic acids or other reagents from the synthesis. The lack of H-e and H-g signals makes it impossible to determine the Au-S bonding effect or the differences between the two sulfur atoms upon Au bonding.

2.4.3.4 Characterization of Core-ligands interactions in Plasmonic gold nanoparticles by Infrared spectroscopy.

IR spectrum of plasmonic NPs is shown in Figure 2-13b and compared with molecular like $Au_{22}LA_{12}$ IR spectra NCs in Figure 3-13a. IR spectrum of the SP NPs showed similar features with the $Au_{22}LA_{12}$ NCs.[30] The similarity in IR spectrum suggested the ligand-core interactions of the SP NPs synthesized are similar to the earlier reported NCs.

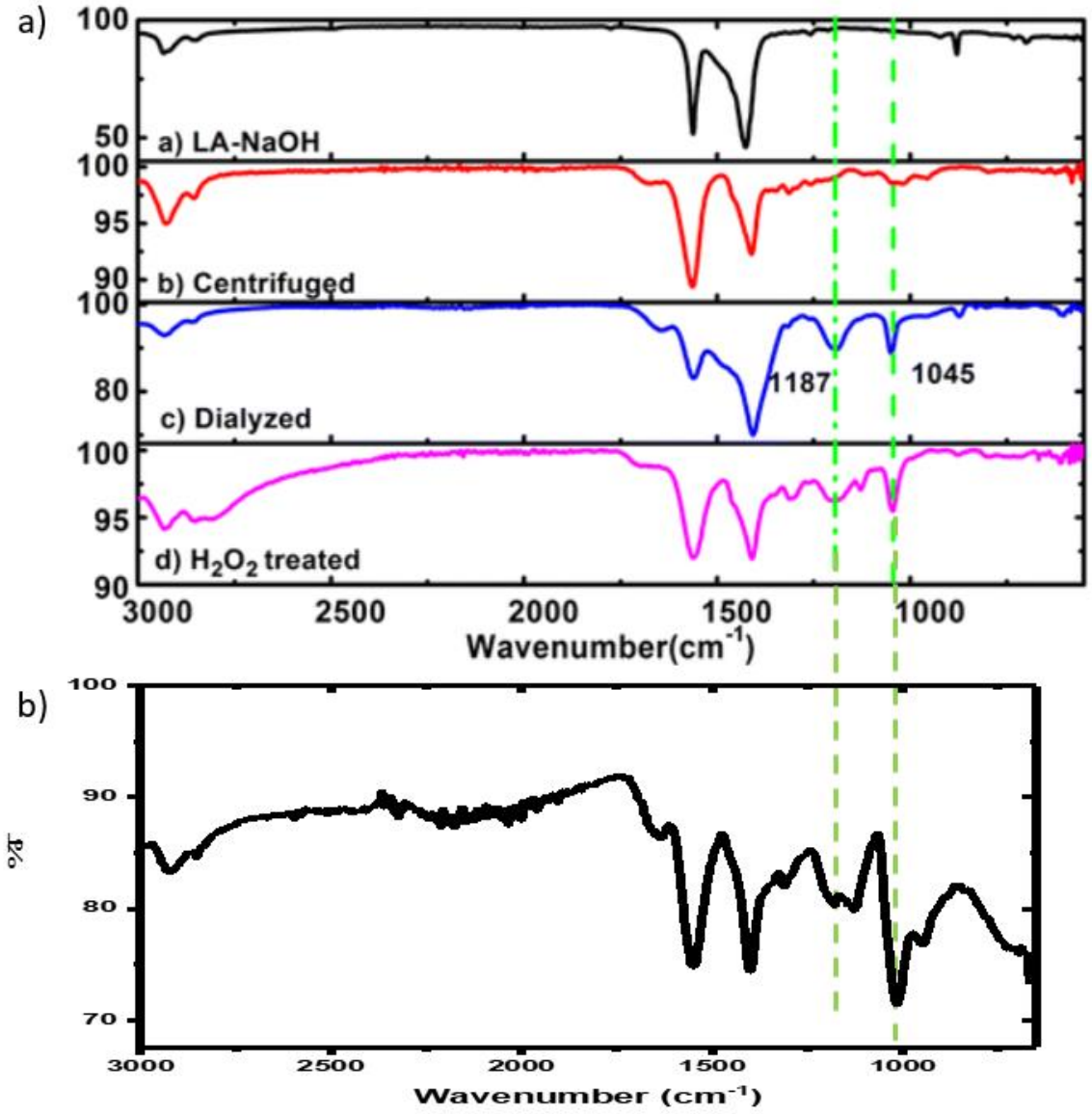

Figure 2-13 Comparison between Au-LA NCs a) FT-IR measurements of the non-oxidized and oxidized $Au_{22}LA_{12}$ clusters. Adapted with permission from J. Phys. Chem. C 2014,

118, 20680−20687. Copyright 2014 American Chemical Society, and b) IR spectrum of plasmonic NPs. Spectrum was recorded by the drop-cast sample after air-dried. The broad features around 3000 cm^{-1} are affected by hydrogen bonding from H_2O.

The lack of S-H stretching signal at around 2500 cm^{-1} determined the purity of the NPs. There is no LA leftover or absorbed onto the ligand. All sulfur atoms in the ligand were either bond to gold or were oxidized. The two distinct peaks at 1187cm^{-1} and 1020cm^{-1} represent the S=O symmetric and asymmetric stretching bands. The double splitting of those two peaks was explained in the supporting information as the on-going oxidation process of the ligands. The two IR signals above clarify the core-ligand interaction bonds. Sulfur atoms of the LA ligands bond to the gold core and some of them are oxidizing to form the SO_x as mentioned earlier.

One significant and exciting difference here is the presence of those two peaks, even though the SP NPs were purified with the ultracentrifuge method. As reported earlier for Au-LA NCs, the sample purified via ultracentrifuge method will be less exposed to oxygen and less oxidized, therefore there is no S=O signal in the IR spectrum.[30] It is not the case here with the SP NPs, even though ultracentrifuge was the only purification method used for SP NPs samples. It seems like the SPR improved the oxidation process more than the NCs samples.

Besides the previously stated, all other signals were similar to $Au_{22}LA_{12}$ which indicated the same core-ligand interaction. The carbonyl stretching at 1690 and asymmetric/symmetric carboxylate stretching at 1560/1405 cm^{-1} were also explained in $Au_{22}LA_{12}$ reported.[30]

2.5 Conclusion

1: 0.39-mole ratio of Au to LA was found to synthesize the smallest nanostructure that support the surface plasmon properties in Au-LA NPs. The composition of this NPs has not been fully clarified by mass spectrometry. Spectroelectrochemistry analysis of the NPs showed similar absorbance changing trend in both positive and negative electrolysis. However, carefully

investigating the change of absorbance spectra pointed out some differences in peaks and valleys between positive and negative scan. It seems 200mV and -200mV is the interesting turning point with the isosbestic point at the 520nm plasmonic band. IR spectrum clarified the ligand-core interaction as well as the oxidation of sulfur atoms in the ligands. However, the broader NMR spectrum limited the investigation of the ligands composition and identified which sulfur was attached to the gold core and which was oxidized.

3 MOLECULAR-LIKE LIPOIC ACID STABILIZED GOLD NANOCLUSTERS

3.1 Abstract

Aqueous nanoclusters, due to the ultra-small size and water-soluble properties, are promising novel materials in sensing, imaging, drug delivery, and other biological and medical applications. Different nanocluster compositions have different properties which might give rise to advantages or suitability in specific applications. Unfortunately, there are not many uniform nanoclusters available due to the difficulty of the synthesis in aqueous environment compared to organic solvents. Considering the inertness of bulk gold or nontoxicity, synthesizing new gold nanoclusters and characterizing the physicochemical properties are fundamentally important. In this work, unique multidentate ligand lipoic acid was used to synthesize new water-soluble gold nanoclusters with molecular energetics. Two different purification methods resulted in two related samples with different features. One has new discrete absorbance bands corresponding to the electronic transitions in UV-visible-near IR spectrum window. The other sample is formed from the first one after a gradual change due to partial oxidation. The other sample is more oxidized with about tenfold enhancement in photoluminescence which is an excellent development for potential biological imagining applications. Common analytical methods such as UV-Vis absorption, photoluminescence, IR spectroscopy, NMR and electrochemical techniques were used to characterize the composition as well as properties of the clusters. The synthetic parameters are optimized based on those characterizations as feedbacks. Also, the Spectroelectrochemical analysis was performed to investigate detailed electronic transitions leading to the electrochemical and optical features. Finite changes around the distinct absorbance bands were also noticed upon oxidation or reduction controlled by electrode reactions. Finally, the thermal treatments with excess MonoThiolate and DiThiolate are found to enhance the

photoluminescence by 2-3 folds. Surprisingly, excess DiThiolate during the thermal treatment increases the electrochemiluminescence (ECL) signal by at least 30-fold. With the high luminescence, ultra-small size, water-soluble features, the new gold nanoclusters have great potential in sensing, and biological imaging and biomedical applications though further theoretical and experimental studies are necessary.

3.2 Background and strategy

Noble metal nanoclusters have drawn tremendous research attention due to their unique properties.[2, 26, 46] Having the core sizes smaller than 2nm, NCs are often atomically precise in chemical composition and have quantized energy levels giving rise to molecular-like discrete absorbance bands in UV-Vis spectra.[19]

Gold nanoclusters have abundant energy states supporting different electronic transitions which correspond to distinct electrochemical and optical features. All factors such as core size, core shape/structure, ligand molecular structure and monolayer composition define different NCs, thus each NCs will have unique properties.[45] Therefore, synthesis of new nanoclusters and understanding their electrochemical, optical, magnetic, catalytic and other physicochemical properties are the prime interest of chemists.

A unique property of gold-thiolate nanoclusters is the luminescence in near infrared spectrum range which is highly favorable for bioimaging due to less interference. The ultrasmall regime (smaller than 2nm), stability and hydrophilic properties offer additional advantages for biological imaging and sensing applications.[47-48] However, one of the significant limits is the relative low photoluminescence quantum efficiency; which hindered the practical applications. The near-IR emission is featured by large Stokes shift and long lifetime and attributed to surface states which might arise from hybridized atomic orbitals of Au and S.[30]

In the motivation of developing new aqueous nanoclusters, the previous synthesis procedure of $Au_{22}LA_{12}$ NCs reported by our group was followed with some modifications.[30] New LA stabilized Au NCs in the molecular like regime was synthesized with finetuned LA ratio (1.7X compare to Au mole). The newly synthesized sample was purified by two different methods. First, the ultracentrifuge purification method resulted in the sample displaying unique and distinct absorbance bands at 500nm, 590nm, and 680nm, which strongly suggest the monodispersity of this new nanocluster. Near-IR photoluminescence is observed with a peak intensity at 775nm. The photoluminescence QE is similar to other aqueous soluble nanoclusters at around 1-2%. The absorbance bands are distinct, unique and entirely new. However, these bands tend to get less intense associated with the gradual oxidation of some ligands. The oxidation process can be suppressed by immediately purging the sample with argon right after ultracentrifuge purification, but it also stops the increase of the luminescence QE.

The second purification procedure adopts dialysis over several days. The photoluminescence QE increased by tenfold from 1% to 10% compared to the sample from ultracentrifuge purification. after the dialysis, all absorbance bands diminished. The newly purified nanoclusters were characterized by conventional analytical methods such as NMR and IR spectroscopy. FT-IR spectra clearly showed evidence of S=O symmetric and asymmetric stretching bands indicating the oxidation of the ligands.

To better understand and actively control the ligand oxidation at the core-ligand interface, and to improve the nanocluster energetics for better luminescence properties, the NCs were annealed at elevated temperature with excess MonoThiols or DiThiols. The Dithiols ligand was used to anneal the NCs into a reduced form of Lipoic acid. The NCs hopefully will be more stabilized and uniform. The photoluminescence spectroscopy was the primary method to

determine the stopping point as well as the success of the annealed method. All annealed sample was purified by the ultra-centrifuge method. IR and NMR spectra of the annealed method were performed to analyze the composition features of the annealed sample. Beside photoluminescence, electrochemiluminescence (ECL) method was used to investigate the luminescence of the annealed sample further.

3.3 Experimental details

The new molecular like Au-LA clusters were synthesized following a previously published report with some modifications.[30] First, the stock aqueous LA solution was prepared by dissolving 15.75mg of lipoic acid (LA) in 12mL of nanopure water. Next, 1mL of 0.5M NaOH was added to the lipoic acid solution to completely dissolve lipoic acid. Second, aqueous Hydrogen tetrachloroaurate (III) solution was prepared with 30mg of Hydrogen tetrachloroaurate (III) (with 3H2O) in 12mL of nano purified water. Then, the lipoic acid and gold solutions were mixed at the mole ratio of 1 gold to 1.7 LA. The NCs referred to as Au-LA 1.7 sample pending full characterization. The Au-LA solution was stirred for four hours until solution color or absorbance changes stopped. After four hours of stirring, the Au-LA mixtures, generally known as Au-thiolate polymeric complexes, were reduced by $NaBH_4$. The ratio of sodium borohydride was 5x compare to moles of gold. Finally, the solution was purified via ultra-centrifuge or dialysis. 3500 MWCO filter was used to ultra-centrifuge the sample, while snakeskin dialysis tubing (3500 MWCO) was used to perform dialysis over a period of four days. UV-VIS absorption and photoluminescence spectrum were recorded periodically to monitor the synthesis.

In the annealing experiment, the dialyzed nanoclusters were reacted with excess reduced Lipoic Acid (dithiol) or reduced L-Glutathione (monothiol) under controlled temperature. Tris(2-

carboxyethyl) phosphine (TCEP) to reduced the Lipoic acid into dithiols because disulfide in not reactive.[49] 1mM Lipoic Acid (LA) solution was prepared by adding LA to nanopured water and sonicated to dissolve the solution thoroughly. The pH of the solution was 4.15. After that, the reduction reaction was carried out by mole ratio of 1 LA to 0.4 TCEP. The reduction was completed in 5 minutes. The solution containing reduced LA was directly added to nanocluster sample at a mole ratio of 0.5 Reduced LA to the clusters. The final nanoclusters after annealing were purified by ultra-centrifuge method.

3.4 Results and Discussion

3.4.1 Gold Lipoic Acid nanoclusters synthesis process monitored by spectroscopy and parameter optimization

Information during the synthesis process is critical in optimizing the sizes and size distributions of the final NCs. Optical features at key synthetic steps were recorded and presented in figure 3-1 to 3-4. Figure 3-1 shows the absorbance spectra at different synthesis steps and reveals the sharp transition from Au-LA complex mixtures to the formation of the NCs after the addition of the reductant. The most obvious changes in absorbance spectrum are the curvature and the increase of a broad band around 400-600nm.

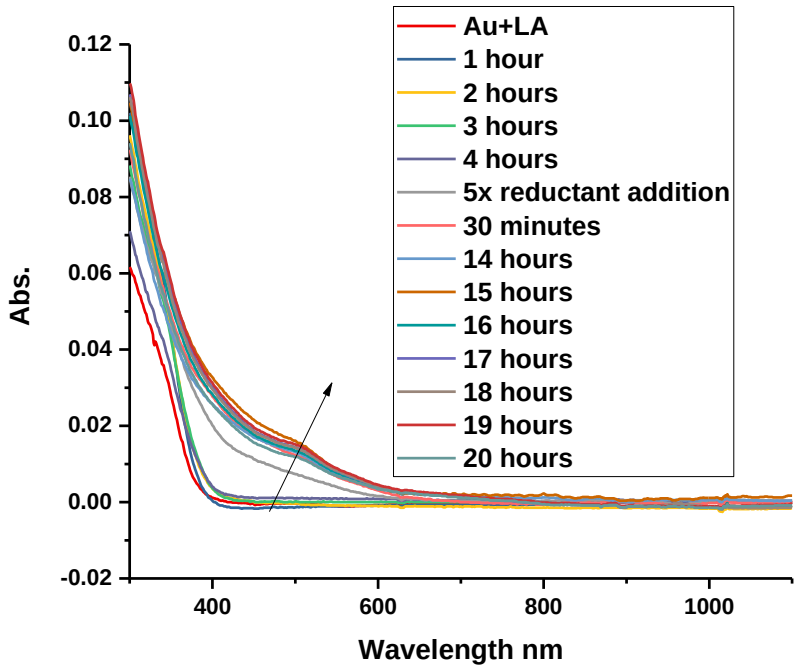

Figure 3-1 Absorbance spectra during the synthesis of the molecular like nanoclusters. Arrow indicates the increase in time/process.

.

Figure 3-2 shows absorbance spectrum details of Au-LA mixtures at different times periods prior to reductant addition. Note that figure 3-2 is the zoom in on the bottom curves in figure 3-1. The color of the mixture solution changed graduated from light yellow to colorless. The subtle changes at the 300-400nm range indicated by the arrow corresponded to the disruption of five atoms disulfide ring of LA. Note the spectra were collected directly from the synthesis mixture without purification. Therefore, the baseline or reference could shift which cause the normalized absorbance to appear negative. Four hours of stirring was picked for this synthetic step because the absorbance spectra stabilized from three to four hours. The mixture did not have photoluminescence during this four hours of stirring.

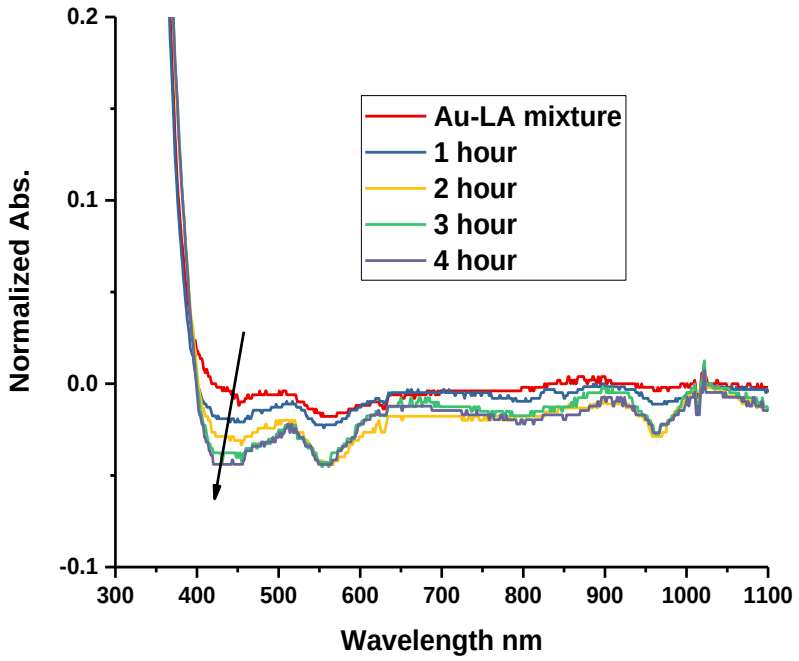

Figure 3-2. Absorbance spectra of Au-LA mixture at different time points. Red curve showed the spectrum of the Au-LA right after they were combined. Blue, yellow, green and grey curves are absorbance spectra of the Au-LA mixture after vigorously stirring collected at 1, 2, 3, 4 hours respectively. The black arrow showed the trend of the changing. The spectra absorbance at 300 nm were normalized to one.

After reductant addition, the mixture solution color changes quickly to dark brown. Accordingly, the sharp decrease in absorbance of the pre-reduced mixture up to 400 nm changes into a more gradual decay toward longer wavelength. There is an increase in the absorbance in 400 to 600nm range with a somewhat distinct shoulder around 500 nm as shown in figure 3-3. Those absorbance features are characteristics of the conversions of Au-thiolate oligo-polymers (Au-SR complexes) into small nanoclusters (with a metal core).

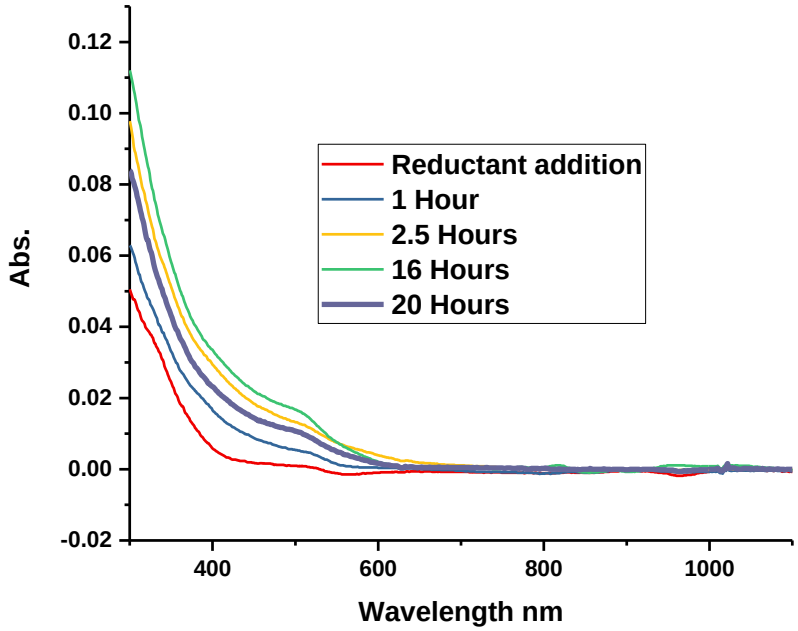

Figure 3-3. UV-Vis spectra of Au-LA mixture after reductant addition. Red curve showed the spectrum of the Au-LA right after the addition of 5x reductant. Blue, yellow, green and grey curves are absorbance spectra of the reduced Au-LA mixture vigorously stirring at 1, 2.5, 16, and 20 hours respectively. The black arrow showed the trend of the changing. Thicker line was used to highlight the final curve.

Photoluminescence can be detected immediately after the mixture was reduced by the 5x reductant. The broad emission spectrum is in near IR region. Overtime the emission intensity increases and stabilizes after 14 hours as shown in figure 3-4. There is not much difference in photoluminescence between 14 hours and 20 hours after reductant addition. The emission could decrease after 20 hours (results not shown). Sixteen hours of stirring after reductant addition was picked to finish the synthesis because of the highest photoluminescence after dialysis purification. At that time point, the three absorbance peaks are also most distinct from the sample isolated by ultra-centrifuge purification.

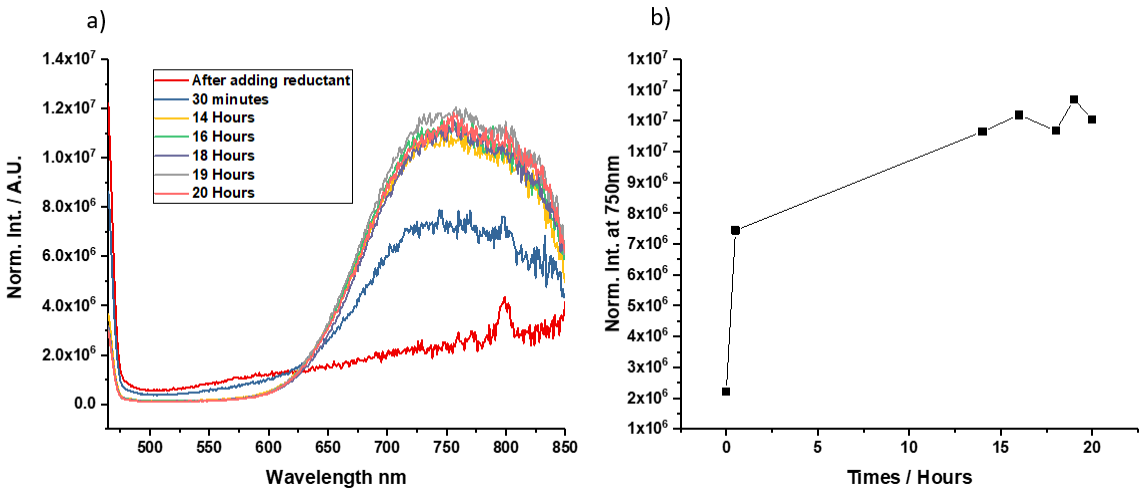

Figure 3-4 a) Photoluminescence spectra during reduction. Photoluminescence spectra were normalized by the absorbance at the excitation wavelength of 400 nm. b) corrected/normalized photoluminescence intensity at emission peaks 750nm.

3.4.2 Optical features affected by different purification methods.

Nanoclusters purified by different method results in different optical features. These features reveal the electronic transitions or energy states of the NCs. Figure 3-5 compares the absorbance spectra of NCs samples purified by different methods. Retrospectively, the results suggest new routes to improve the sample, i.e. monodispersity or size, and the related properties.

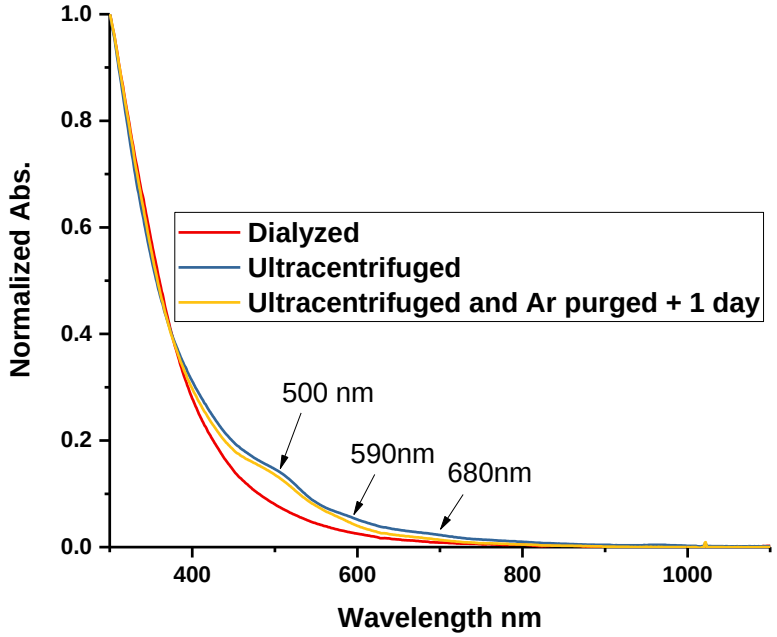

Figure 3-5 Normalized absorbance spectra of nanocluster using different purification methods. The absorbance spectra were normalized at 300nm.

For the first time, Au-LA nanoclusters with multiple distinct absorption bands at 500nm (2.48eV), 590nm (2.10eV), and 680nm (1.82eV) were obtained via ultra-centrifuge purification. These unique and distinct bands suggest high monodisperse of a new nanocluster. Each absorbance band suggests electron transitions from lower to higher energy states. However, these bands become less distinct under ambient condition. Those absorption bands can be conserved by purging the nanocluster solution with Argon as shown. The results suggest the oxygen effects specifically the oxidation of some ligands later characterized by vibrational spectroscopy. Similar trends have been observed in our earlier report of Au22LA nanoclusters.[30]

The absorbance spectrum of the dialyzed sample shows featureless decay in the whole range. The loss of the distinct bands and steeper decay curvature is attributed to the much longer exposure to oxygen with the synthetic mixture during dialysis compare to ultracentrifuge. There

is a tradeoff between this loss of the absorption bands and the increase in photoluminescence resulted from the oxidation process. Figure 3-6 showed the normalized photoluminescence spectra collected from the same synthesis batch but using different mentioned purification methods.

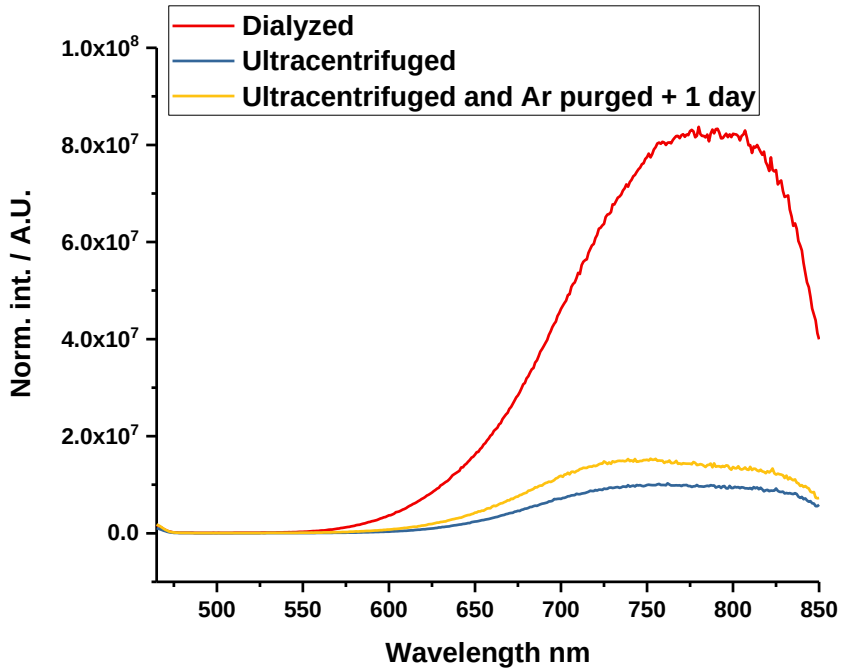

Figure 3-6 Normalized luminescence spectra of the same batch NCs using different purification method. Each spectrum was divided by the absorbance at 400 nm from the same solution to one. In other words, the concentration of different samples were normalized to be the same.

Dialysis purification delivers nanoclusters with a quantum efficiency ten times higher than the ultra-centrifuge method. It is a unique feature only observed in our Au-LA NCs. From same synthesis batch which showed less than 1% QE before purification, half was purified via ultra-centrifuge showed a small increase in QE from 1% to 2%. A mentioned above, the absorbance band is stronger from 400nm to 700nm prior to purification and shows three distinct peaks at 500nm (2.48eV), 590nm (2.10eV), and 680nm (1.82eV) afterwards. These distinct

peaks are unique for this 1.7 Au-LA NCs and indicates high uniformness. Without Argon purging, these bands will gradually disappear along with the increase in the photoluminescence QE, but it will never reach the photoluminescence intensity from the dialyzed sample. This phenomenon might be due to the annealing effect during the dialysis process while NCs still surrounded by excess ligands discussed in later section. The other half of the same batch was purified by dialysis. The absorbance peaks disappeared while the QE increased ten times from 1% to 10%. This increase matches well with what reported earlier in $Au_{22}LA_{12}$ NCs.[30] The enhancement in QE will strengthen the applicability of the NPs in sensing and bioimaging purpose which is a significant feature for water-soluble NPs.

3.4.3 Impact on optical features by the variation of Lipoic acid ratios to Gold

Similarly shown in Chapter 2, different mole ratio LA to Au will result in NCs with different average sizes. The products are generally a mixture containing predominantly either thermodynamically stable or kinetically trapped sizes/compositions, or both. In the motivation of the creation of new aqueous NCs which are more monodispersed and have the highest photoluminescence, different ratios of Lipoic acid to gold was investigated. Figures 3-7 showed the absorbance, and photoluminescence features of the NCs synthesized from different Au-LA ratios.

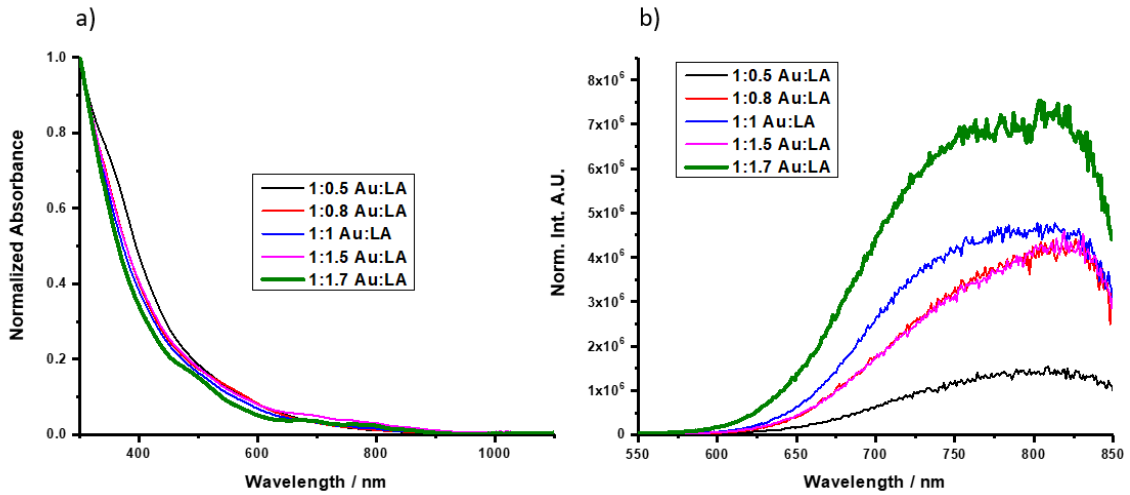

Figure 3-7. a) absorbance and b) photoluminescence spectra of NCs synthesized from different Au-LA ratios. The absorbance spectra were normalized at 300nm. The photoluminescence spectra in b were excited at 400 nm and normalized by absorbance value at 400nm.

As mentioned earlier in Chapter 2, starting from Au-LA 1-0.5, the resulting sample started to have NCs features. The Au-LA 1-0.5 sample was starting to show weak photoluminescence signal with featureless decay absorbance. The photoluminescence of higher LA ratios showed an increase in intensity, including few bumps on absorbance spectra. At Au-LA 1-1.7 (bold green) the highest photoluminescence was reached, and the distinct absorbance bands were the most intense. At higher LA ratios to Au (2.0 or 2.5) (not shown) there is no change in photoluminescence intensity, and the absorbance spectra only have 505nm bands, indicating the known $Au_{22}LA_{12}$ sample.[30] Therefore the Au-LA 1-1.7 ratio was picked as the standard synthesis condition

3.4.4 Impacts on optical features by the variation of reductant ratio

To optimize the synthesis for improved properties such as stronger photoluminescence or better-defined absorption bands, different ratios of reductant $NaBH_4$ to Au was investigated and resulted in clusters with different optical properties. With 1x ratio of $NaBH_4$, the clusters display

an emission peak at around 700nm. Higher ratio of reductant results in the clusters with emission peak more red-shifted. The 5x reduction produced the highest QE with the peak in the middle. There is a slight difference in absorbance spectra between samples resulted from different reductant ratio. The sample reduced with a lower ratio of reductant had absorbance spectrum with steeper decay curvature as shown in figure 3-8 a. The excitation spectra of those samples are shown in Figure 3-8 c. In general, the excitation spectra of all Au-thiolate nanoclusters are similar in shape. Unlike small molecules, the excitation and absorption details does not have a clear correlation. With significant Stokes shift as a common feature, the emission spectrum shape is also independent with excitation energy (at room temperature). The 5x ratio of reductant w.r.t. gold was picked as standard synthesis condition to achieve the highest photoluminescence intensity.

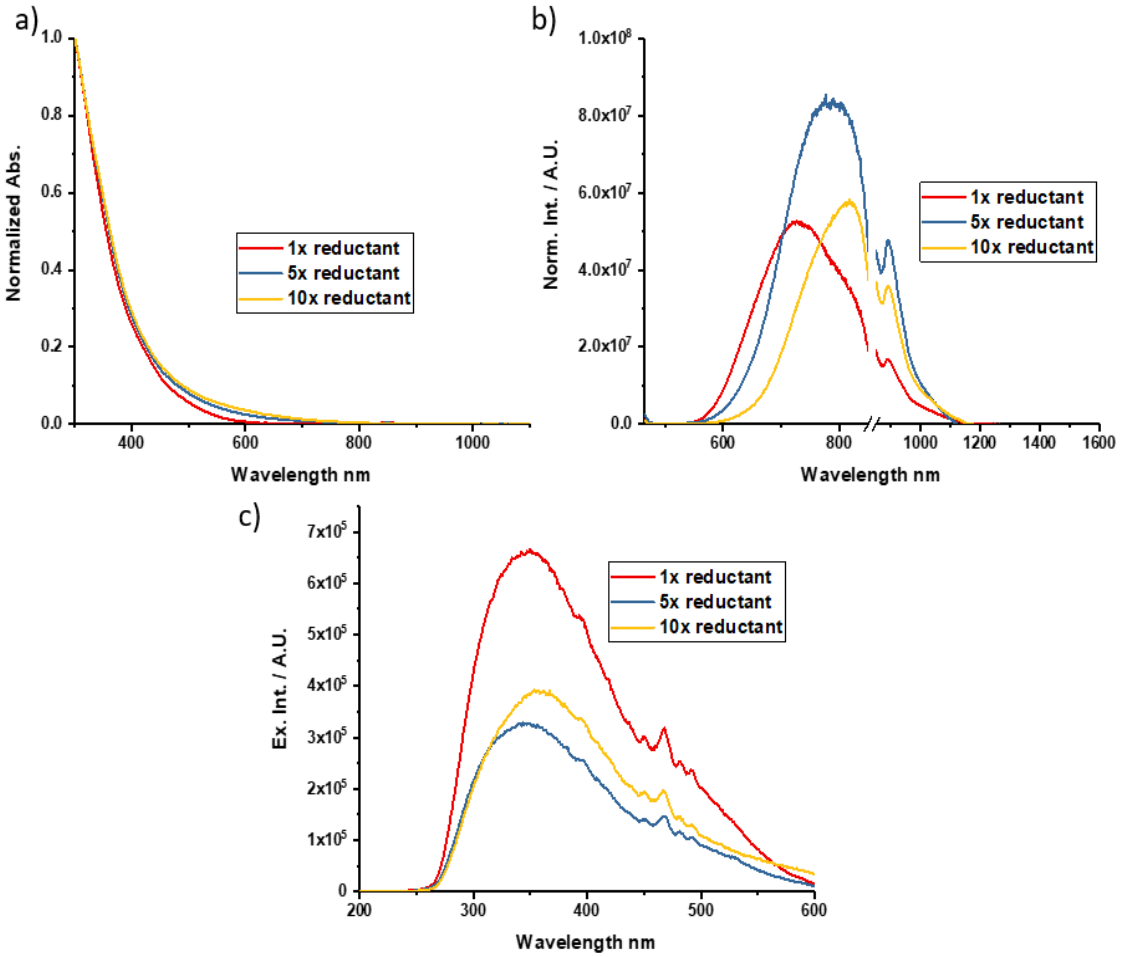

Figure 3-8. a) Normalized Absorbance spectra b) Normalized corrected photoluminescence spectra and c) excitation spectra of molecular like nanoparticles with different reductant (1x, 5x and 10x) ratio compared to a mole of Gold. 1.7X LA:Au. All NCs were purified by dialysis method. The absorbance spectra were normalized at 300nm. The photoluminescence spectra in b were excited at 400 nm and normalized by absorbance value at 400nm. The break on wavelength axis separates the response from two different detectors in luminescence spectra in b. Raw data of excitation spectra were shown in c, the detection was at peak of the emission spectrum for each sample (1x was at 730nm, 5x was at 780nm, and 10 was at 820nm).

3.4.5 Oxidized sulfur identified by Infrared spectroscopy

Infrared spectroscopy is used to understand the core-ligand interaction specifically via Au-S bonding. Figure 3-9 shows the comparison of IR spectra between the nanoclusters purified via two different methods: a) ultra-centrifuge method versus b) dialysis method. The IR spectrum

of the plasmonic NPs discussed in chapter 2 is also shown as c. Firstly, the lack of S-H vibration band (at around 2500 cm^{-1}) in all spectra confirmed the ligand bind to the gold core by Sulfur atoms. Other major features identical to free LA ligands include the 1690 cm^{-1} from carbonyl stretching, and the 1560 and 1405 cm^{-1} from asymmetric and symmetric stretching of carboxylate. These peaks could interchange under different pHs.[30]

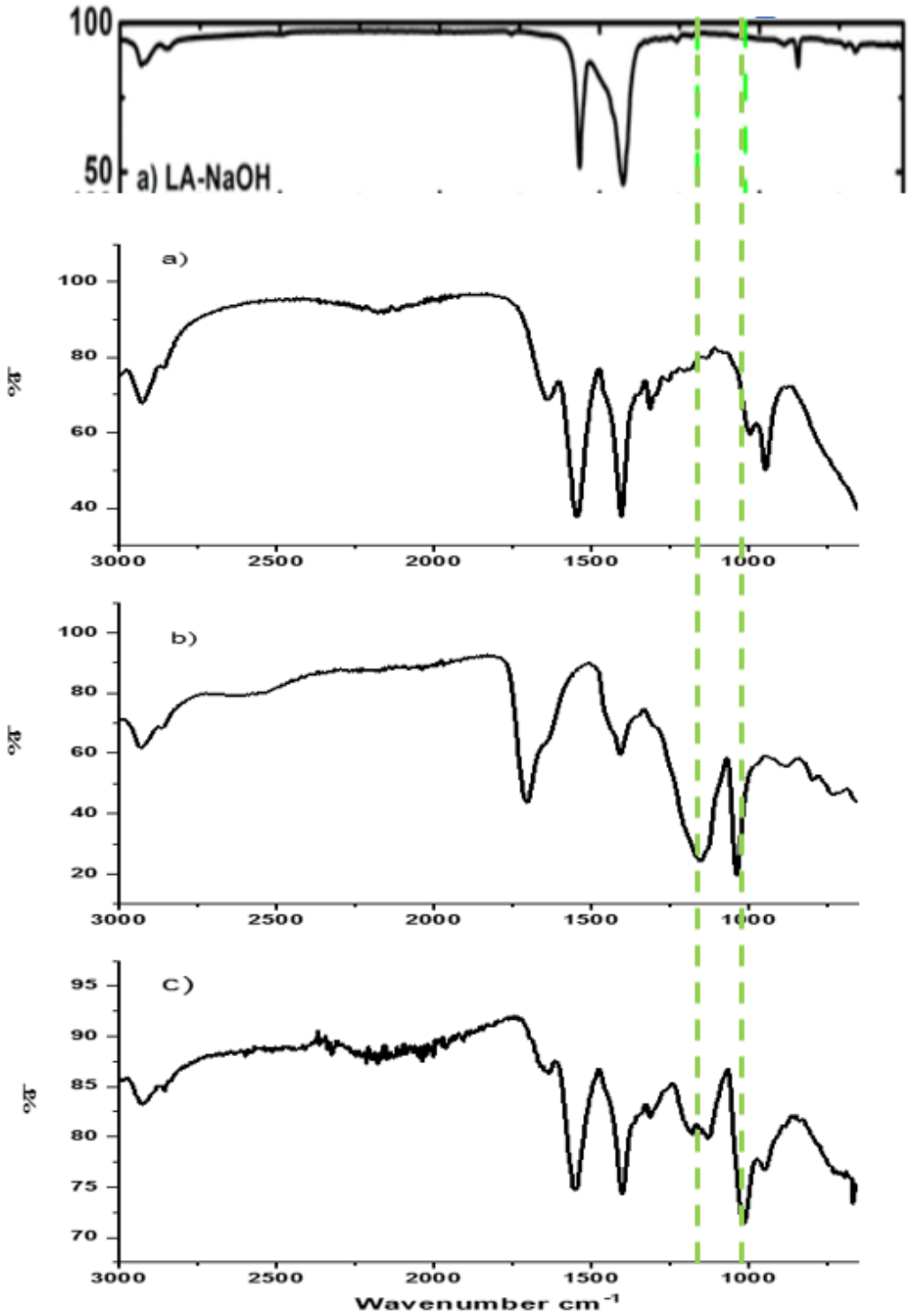
100
50
a) LA-NaOH
a)
b)
c)
%
Wavenumber cm-1

Figure 3-9 FTIR spectra of a) molecular like NCs by ultra-centrifuge, b) molecular like NCs by dialysis and c) Plasmonic NPs. Each spectrum was recorded by drop-casting the sample and air-dried. The broad features around 3000 cm^{-1} are affected by hydrogen bonding from H_2O. Top panel is FTIR spectra of Lipoic acid for reference.

Two sets of new distinct peaks ultimately stabilized at 1045cm^{-1} and 1187cm^{-1}, which were not present in IR spectrum of LA itself, are S=O symmetric and asymmetric stretching bands. The spectrum feature clearly confirms the gradual sulfur oxidation (i.e. -SO, -SO2, -SO3). In the dialysis samples, these two peaks are a lot more prominent. In the ultracentrifuge sample, there is no peak at 1187, and the peak at 1003cm is weaker. The results indicate there are less oxidized sulfurs, either happened during the IR data collection or during ultracentrifuge, or both. In previous work on the $Au_{22}LA_{12}$ NCs, determined by combined IR and NMR analysis, in six out of the twelve LA ligands, one sulfur bond to Au, and the other was oxidized. The rest sulfur atoms (18 remaining ones) were not oxidized and bond to Au directly. We believed the same concept is applicable in this new nanocluster, but quantitative understanding requires further analysis.

3.4.6 Ligand composition by NMR

IR spectroscopy clearly revealed the oxidation of some sulfur atoms in ligand monolayer qualitatively. The next question is the specific location of oxidized sulfur. ^1H NMR Spectra of the 1-1.7 Au-LA NCs and disulfide lipoic acid in D_2O as well as the molecular structures were provided in figure 3-10. As seen in most nanocluster ^1H NMR Spectra, the peaks of those protons close to Au surface are significantly broadened known as line broadening effect. The broader peaks in the Au-LA NCs spectrum, compare to free Lipoic acid spectrum, confirm the formation of the NCs. The lack of sharp peaks also confirms the efficacy of purification methods to remove unbound lipoic acids in the solution. The signal at α-position from S will be shifted

upon bonding to Au and more broadened due to more significant motion restriction and heterogeneity in the neighboring chemical environment.

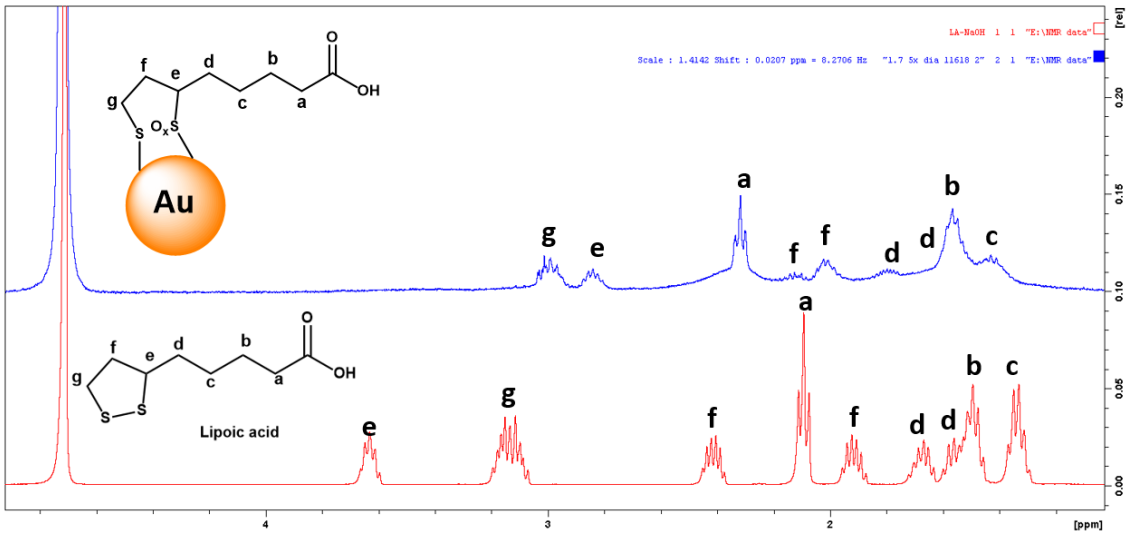

Figure 3-10 1D ^{1}H NMR spectra of Lipoic Acid compare with Au-LA NPs in D_2O with solvent peak at 4.80ppm. The NCs structure is only one in three possible structures.

The chemical shift of H at carbon positions g and e will be the key signals to evaluate the sulfur bonding or oxidation. The signals are however significantly affected by line broadening effect which make the direct peak assignment challenging in ^{1}H NMR spectrum. Therefore, 2D COSY NMR spectra as shown in figure 3-11 are necessary to make the peak assignment accurately.

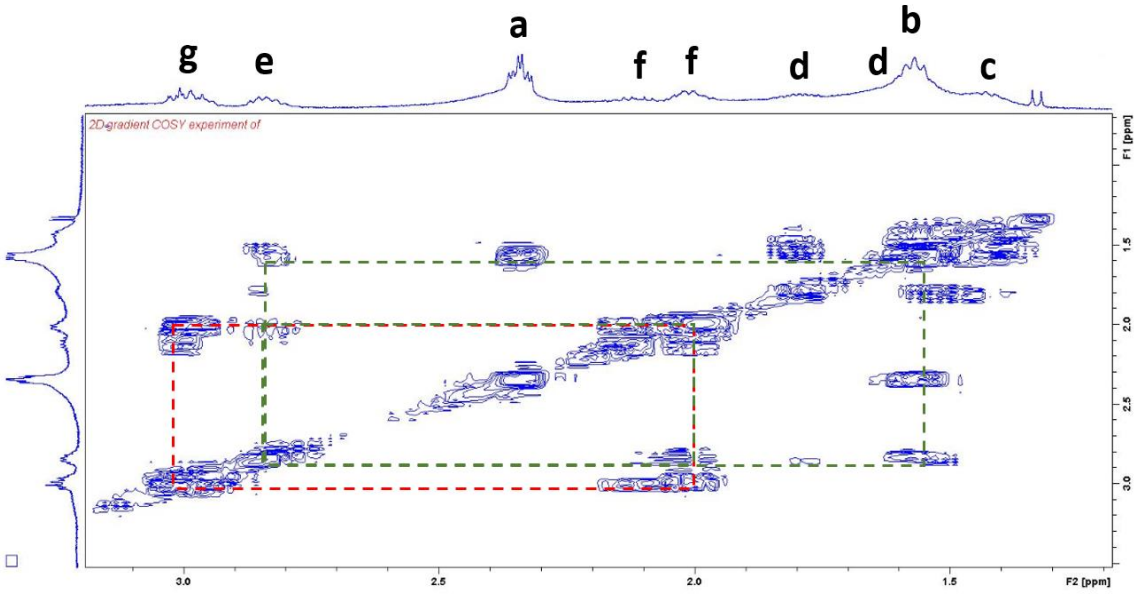

Figure 3-11 The COSY spectrum of dialyzed Au-LA NCs in D_2O with solvent peak at 4.80ppm.

The peak at 3 ppm showed crossed-peaks with H-f signals. Therefore it is assisted to the proton on C-g (H-g). The peak at 2.8ppm with cross-peaks with H-f and H-d signals were assigned to the proton on C-e (H-e). The signal of H-e was broadened and shifted to more upfiel position indicated the oxidation of the sulfur adjection to it. The inner sulfurs of some ligand were oxidized. The possibility that both sulfurs from one lipoic acid were oxidized is unlikely because the ligand-core interactions would become too weak, causing dissociation of the ligand from Au surface and subsequent cleaning out by the purification process.[30] therefore the Au-LA 1-1.7 are new NC which is different with previous synthesized $Au_{22}LA_{12}$. Figure 3-12 shows the new NC with two possible ligand-core interface structures.

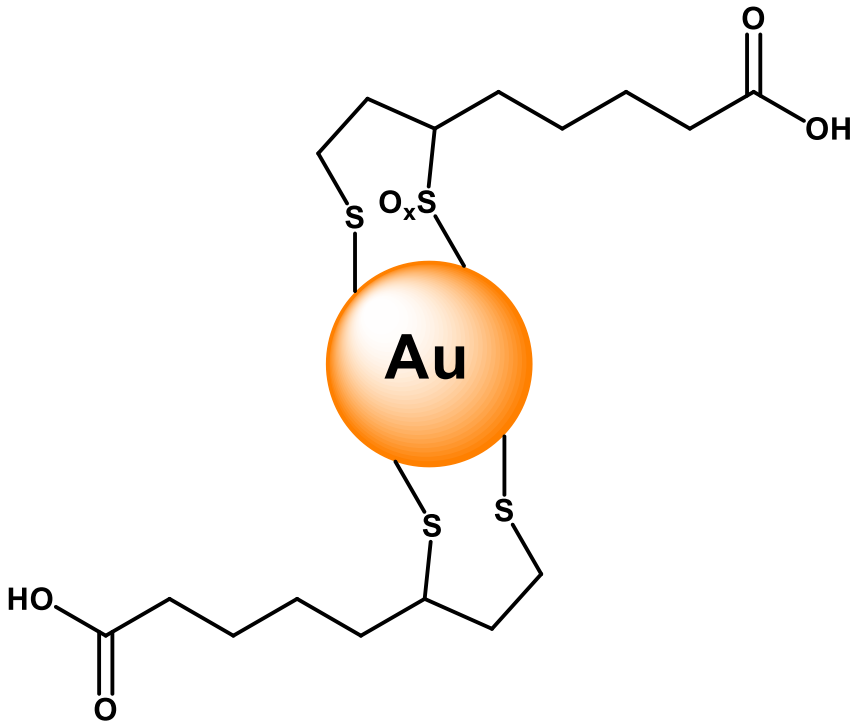

Figure 3-12. Basic representation of Au-LA 1-1.7 nanocluster. Only two different ligand forms are sketched for clarity.

One of the H-f peaks shifted more significantly to the upfield position. The splitting of both H-f including the changes in chemical shift reveal a different chemical environment which supports the bonding of both sulfurs to Au. (58)

3.4.7 Spectroelectrochemical analysis

The three distinct bands in absorbance spectra of the ultra-centrifuged sample, together with their disappearance over time are very intriguing. Each band could correspond to a certain electron transition from lower to higher energy state/s with the same energy difference (electron volt, eV). Further investigations of these bands are necessary to elucidate the detailed energy diagram of the NCs. Two sets of spectroelectrochemistry experiments were performed. After applying either positive or negative potentials to a NCs solution, an absorbance spectrum was

recorded and analyzed at each potential after the charging current decreases below a threshold value (i.e. less than 10%). All electrolysis spectra were subtracted by the original spectrum (prior to electrolysis). The changes in absorbance induced by the applied potentials indicate the enhanced or suppressed electronic transitions of the corresponding energy state/s.

Basic electrochemistry features of the ultracentrifuged NCs measured by CV and SWV are firstly shown in Figure 3-13. More detailed comparison of the more-oxidized and less-oxidized NCs was discussed elsewhere.[50]

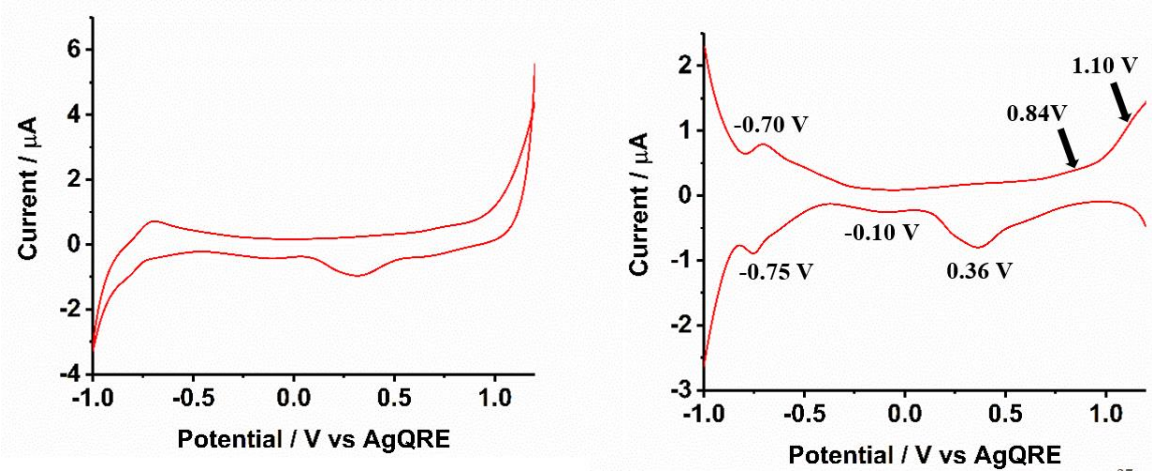

Figure 3-13. CV and SWV of the Au-LA Clusters NCs via ultracentrifuge purification? in H2O. The NCs solution was purged with Ar for 15-30 mins with 0.1 M NaClO4 as the supporting electrolyte. A 0.2 mm platinum disk working electrode, platinum foil counter, and an Ag/AgCl wire were used in all measurements.

Like most aqueous Au NCs, the electrochemistry features are not as impressive compared to organic soluble ones. Though the potential window was limited in water, a few redox activities were observed. In the oxidation scan of SWV, the key features include a peak at -0.70 V, a small shoulder at 0.84 V, and possible another feature at 1.1 V. The two positive potential peaks were believed to be a HOMO state, with spacing of 260 mV. The 0.26 eV charging energy is close to other molecular-like gold nanoclusters in this size range. In the reduction scan SWV, defined peaks at -0.75 V, -0.10V and 0.36V were observed. In reference to the CV curve where a

broad cathodic current and the reversal oxidation around -0.7V can be seen, the peak at -0.75 V is attributed to LUMO. The broad reduction around +0.36 is attributed to the reversal process after the oxidation of HOMO states which is electrochemically irreversible. There is also a possibility that energy or structure relaxation occurred upon oxidation that requires further investigation. A HOMO-LUMO spacing of 1.59 V by electrochemistry is proposed which is in reasonable agreement with the absorption spectrum where the optical gap is around 1.59 eV. The energy gap also aligns with other clusters like the various $Au_{25}SR_{18}$. The potentials around the current valley were used to manipulate electronic transitions in spectroelectrochemistry analysis.

Figure 3-14 shows spectroelectrochemistry results of molecular like 1-1.7 Au-LA NCs purified by ultracentrifuge method. Differential spectra showed major differences between oxidation (top panel) and reduction (bottom panel) electrolysis. Electrolysis under negative potentials made much less difference in the absorbance spectra compared to positive potentials. Within the HOMO-LUMO states, i.e. potential is within +0.84 to -0.75V, there is no accessible states for the AuNCs, no change is expected. With sufficient overpotential to drive the electron transfer reactions at 1.0V and 1.2V, the absorbance spectra showed changes around the three distinct peaks area. A positive differential absorbance means an increase in the corresponding electronic transitions after the oxidation of HOMO electron/s. Interestingly, the original absorption bands are at the valley in the differential spectra. In reference to the irreversible CV features, the oxidation and significantly shifted reversal reduction, it is likely the energy states such as HOMO is shifted upon oxidation. Limited by water splitting, energy states below HOMO could not be accessed which should account for those absorption bands. Increase in absorbance at 3-4 eV range has been observed in several nanoclusters of different sizes and with different thiolate ligands. Those are generally attributed to the electrons at the Au-S bonding and not

specific to a specific nanocluster. Further study is needed to propose a more specific energy diagram. After the conditions to retain those discrete absorption bands are determined, phase transfer into organic phase following our previous reports will allow the access to additional energy states below HOMO and above LUMO, which will reveal different combinations of electron transitions.[50-51]

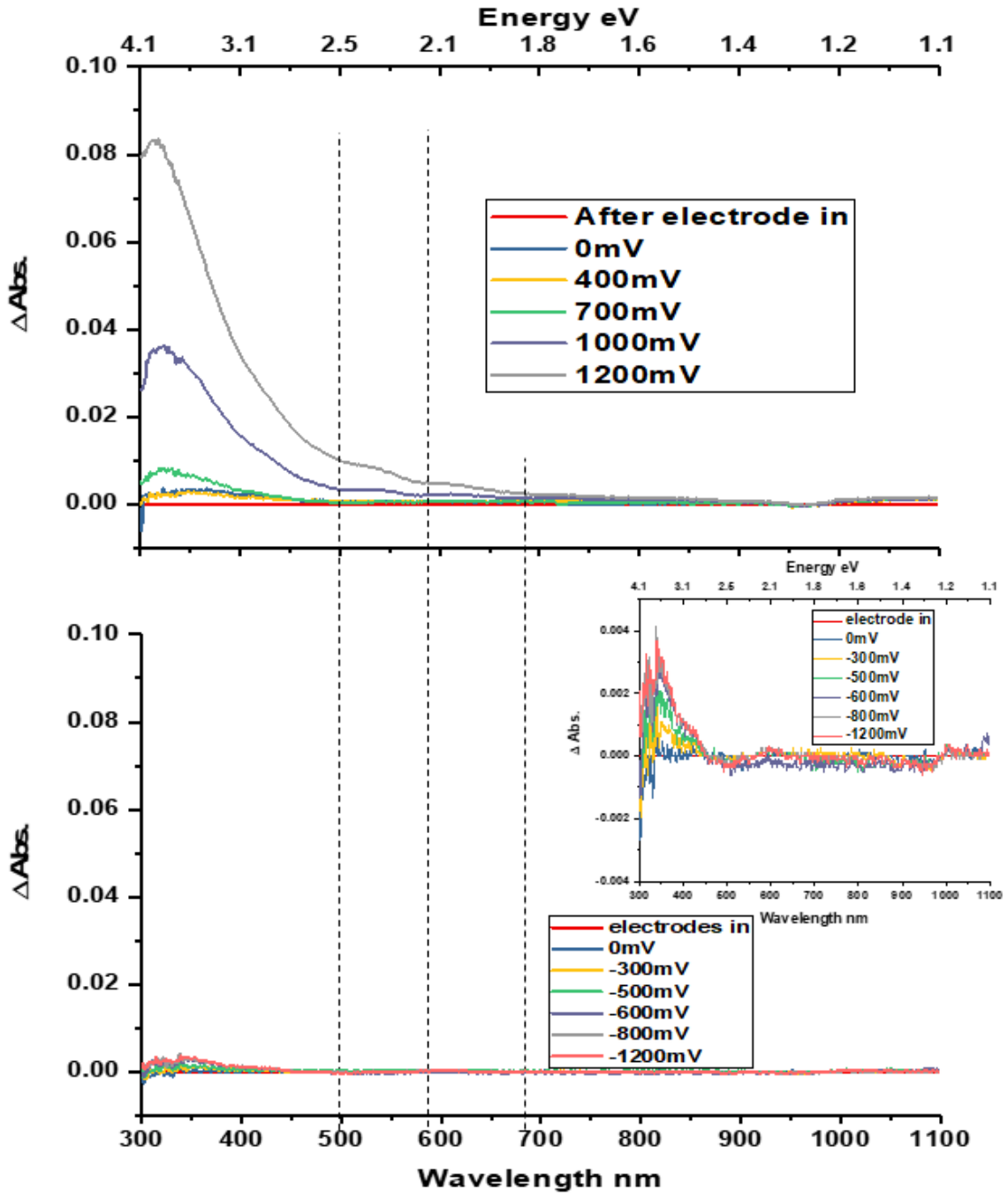

Figure 3-14. Differential spectra of ultra-centrifuged Au-LA 1-1.7 NCs after electrolysis under different potentials. The Au NCs were dissolved in water to have an absorbance at 300 nm around 0.3 with 0.1M $NaClO_4$ supporting electrolyte. The analysis to more positive and negative potentials was performed separately to avoid possible irreversible changes to accumulate over stepwise redox charging. The original spectrum before electrolysis was used as a baseline for subtraction. The vertical dash lines indicate the three absorbance bands in original absorbance spectrum which are 500nm, 590nm, and 680nm respectively from left to right. The changes in absorbance spectra were enlarged in the inset for the bottom panel.

Figure 3-15 provides the original absorbance spectra of the NCs collected in the electrolysis under positive potentials for reference (raw data of Figure 3-12 A).

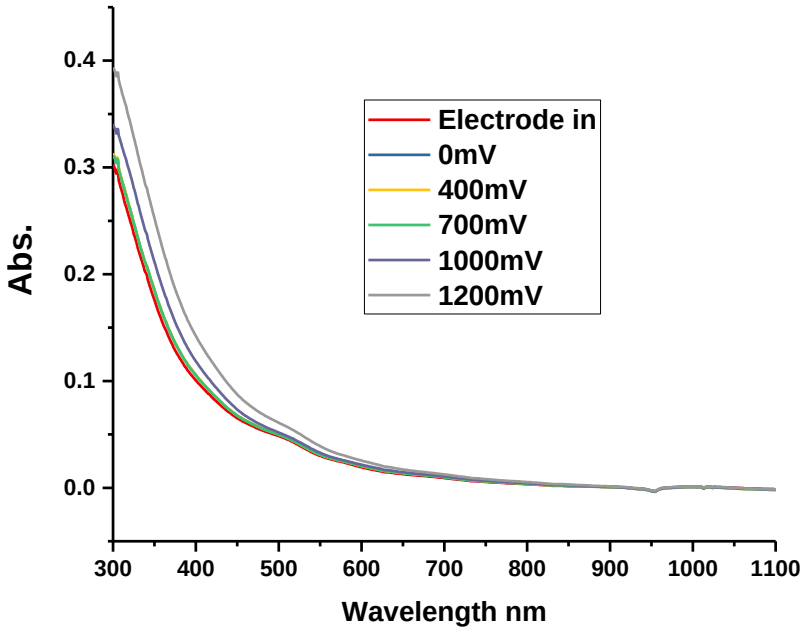

Figure 3-15. Raw data of absorbance spectra of electrolysis scans of molecular like Au-1.7 LA NCs

3.4.8 Heat treatment to enhance photoluminescence.

Tailoring existing NCs is necessary to further improve the monodispersity for broadening the potential applications. One of the most straightforward techniques is annealing, which uses moderate temperature and excess free thiols at a certain ratio to Au NPs. This is also called size focusing because those less stable ones would be decomposed or converted into more stable ones. The process has also been found to enhance the near IR photoluminescence of the AuNCs. Considering the gradual changes during purification process which is passive and poorly

controlled, active annealing is performed to expedite and better control the process. Molecular like Au-LA NCs were annealed separately with MonoThiol (Reduced-glutathione) and DiThiol dihydrolipoic acid (DHLA), which is the reduced form of Lipoic acid. The annealed process was monitored when the photoluminescence reaches maximum intensity before purification by ultra-centrifuge. The purified annealed sample was then studied by analytical analysis with NMR, IR, ECL, and Electrochemistry.

3.4.8.1 Annealing with MonoThiols

After the synthesis and purification via dialysis, molecular like Au-LA NCs were heated at 60^{o}C in water with reduced Glutathione (Glu) at an estimated mole ratio of 1:1 Glu:NCs. UV-Vis absorbance and photoluminescence spectra were recorded during the annealed process for monitoring purpose. The annealing process was stopped when the sample had maximum emission intensity, followed by immediate purification by ultra-centrifuge method and analysis by analytical techniques. The photoluminescence spectra during the annealing process are shown in Figure 3-16, and the normalized intensity at emission peak 800 nm are shown in Figure 3-17.

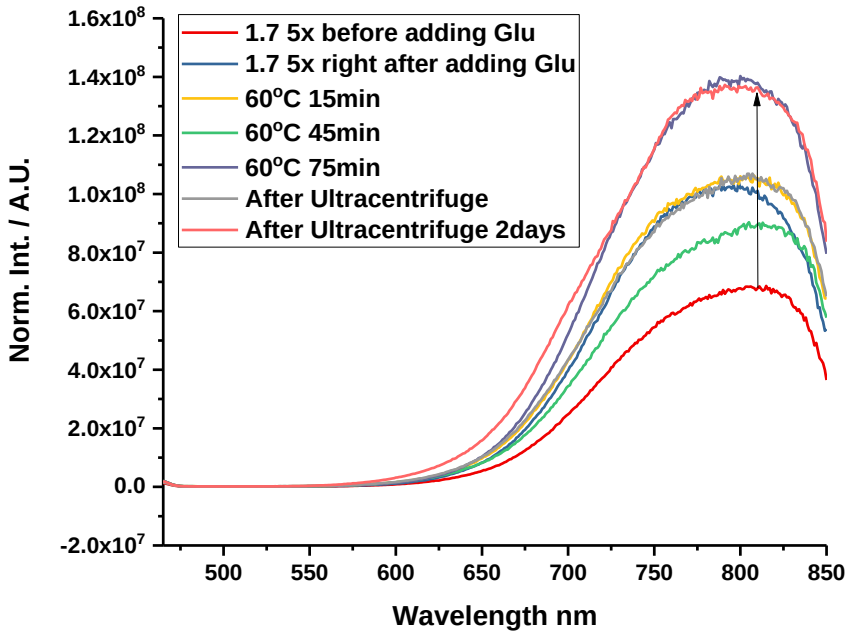

Figure 3-16. Normalized photoluminescence spectra of molecular like Au-LA NC annealed with reduced Glutathione at 60 degrees Celsius. Luminescence spectra were normalized by the absorbance at the excitation wavelength of 400 nm.

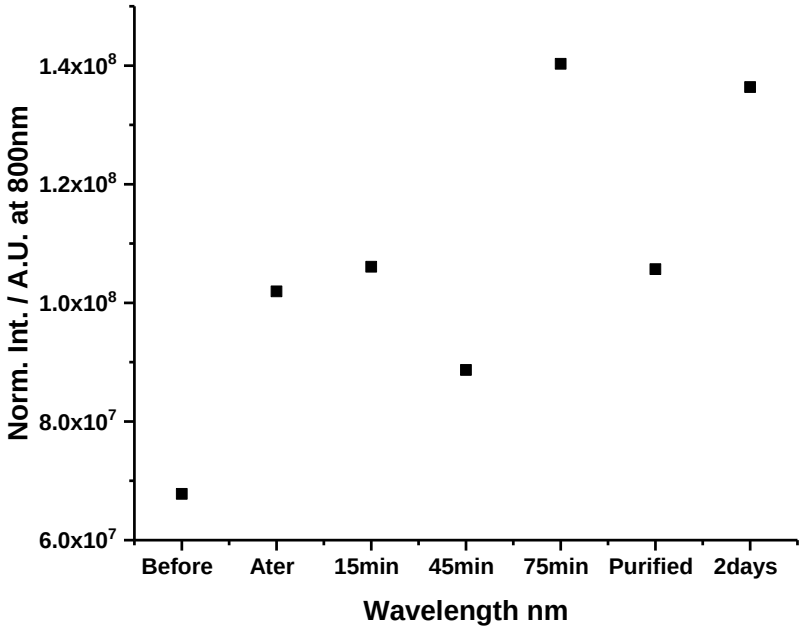

Figure 3-17 Normalized photoluminescence intensity at 800nm at different steps of the annealing process with MonoThiolate reduced Glutathione.

The black arrow indicates the general trend of the photoluminescence increase through the annealing process. UV-Vis spectra show no difference during the annealing process indicating that the core size did not change appreciably. The QE of NCs was around 7% before the addition of reduced Glutathione. Right after the MonoThiolate was added, the QE immediately increased to 11% followed by the decrease to 9% at 45 minutes. The fluctuation is attributed to insufficient mixing and the fast thiolate addition to the ligand monolayer. (cite Zhenghua Tang's Langmuir paper) The emission increased again and reached a maximum at 75 minutes with 15% QE. The annealed NPs were purified by the ultra-centrifuge method to stop the reactions at the maximum QE. There is no significant change or shift in emission spectra's shapes and peaks before and after the thermal treatment. The emission peak is located at

approximately 800 nm and has a small shoulder at 775 nm which remains throughout the heating process.

NMR and IR spectroscopy are employed to characterize the annealed NCs. Figures 3-18 showed 1D proton NMR spectrum of the annealed sample right after purification.

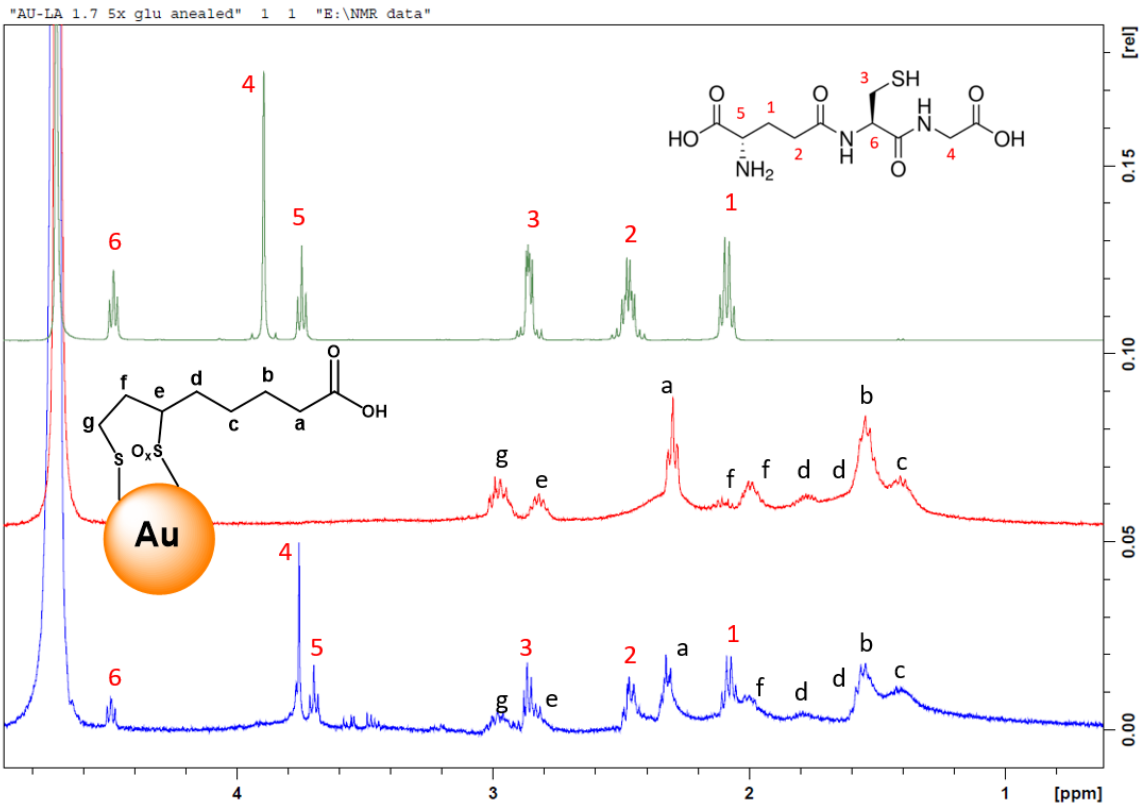

Figure 3-18 H NMR spectra of purified annealed sample compare with Au-LA NPs and Glutathione in D_2O with solvent peak at 4.80ppm.

The spectrum showed a combination of Glutathione and Au-LA NPs peaks. From ^1H NMR spectrum, several peak signals were identified such at H-6, H-4, and H-5 at higher ppm region. Oppositely, H-b, H-c, and H-f also identified at lower ppm region. To support the peak assignment, 2D COSY NMR spectrum is shown in Figure 3-19.

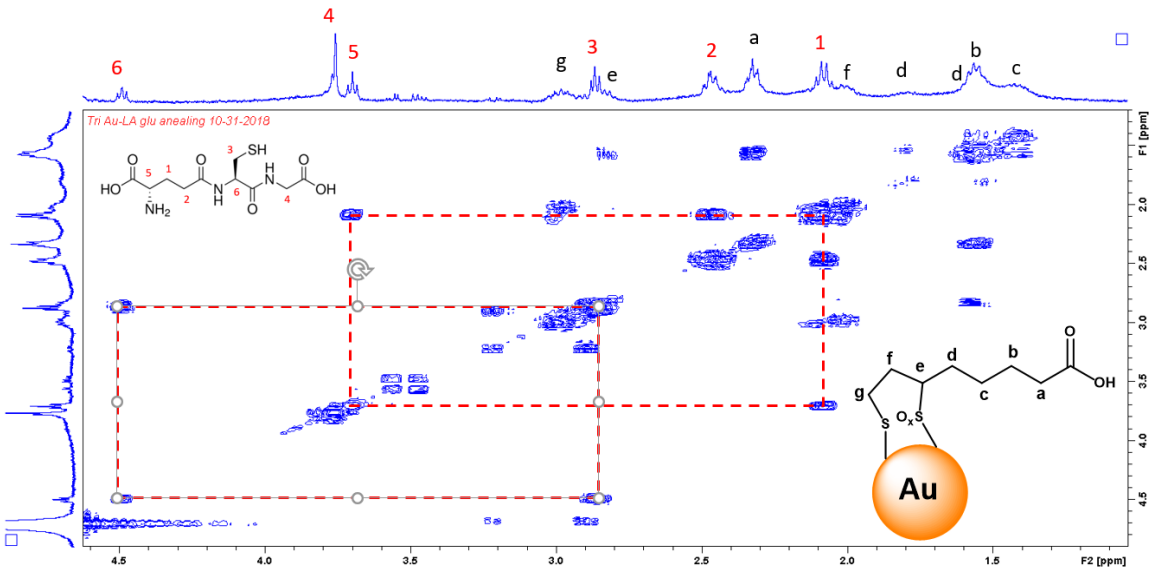

Figure 3-19 COSY spectrum of the purified annealed sample in D_2O with solvent peak at 4.80ppm.

Annealed sample's Glutathione peaks are not broader. The three peaks from the most downfield position belong to Glutathione H-6, H-4, and H-5 respectively. These three peaks are key information to assign more upfield peaks. A cross-peak identifies the H-3 peak with H-6 peak. Similarly, H-1 is clarified by a cross-peak with H-5s, thereby determining the H-2 signal by a cross-peak with H-1. The relative defined, not shifted not broadened. Glu proton signals might suggest a very uniform NC sample which provides uniform chemical environment for the incoming Glu ligands, or the Glu ligands just absorbed onto the monolayer of the NCs.

Though IR is not as quantitative or sensitive, the FTIR spectrum of the annealed sample after purification was shown in Figure 3-20. There is no SH peak at around 2500 cm^{-1} region indicating that there is insignificant amount of free or absorbed Glutathione in the sample.

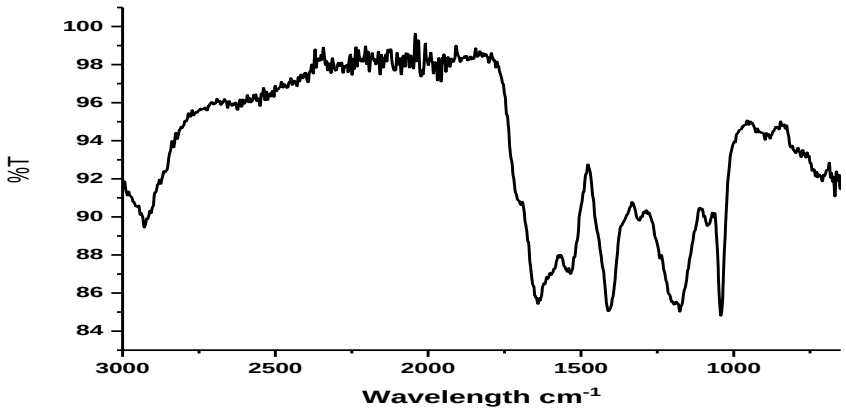

Figure 3-20 FTIR spectrum of the annealed sample after purification. Spectrum was recorded by the drop-cast sample after air-dried. The broad features around 3000 cm^{-1} are affected by hydrogen bonding from H_2O.

There is no difference in ECL and electrochemistry analysis between before and after annealing.

.

3.4.8.2 Annealing with DiThiols

The reduced form of Lipoic acid, dihydrolipoic acid (DHLA), was used to anneal the molecular like NCs. Tris(2-carboxyethyl) phosphine hydrochloride (TCEP) was used to reduce Lipoic to DHLA. Following a previous report, LA acid was reduced by TCEP in water at pH 4.5 within 5 minutes.[49] NMR spectra were taken to guarantee DHLA existed and all TCEP was consumed. Figure 3-21 shows the ^1H NMR spectrum of the LA reduced by TCEP in D_2O. Spectra of LA and TCEP are also provided as references.

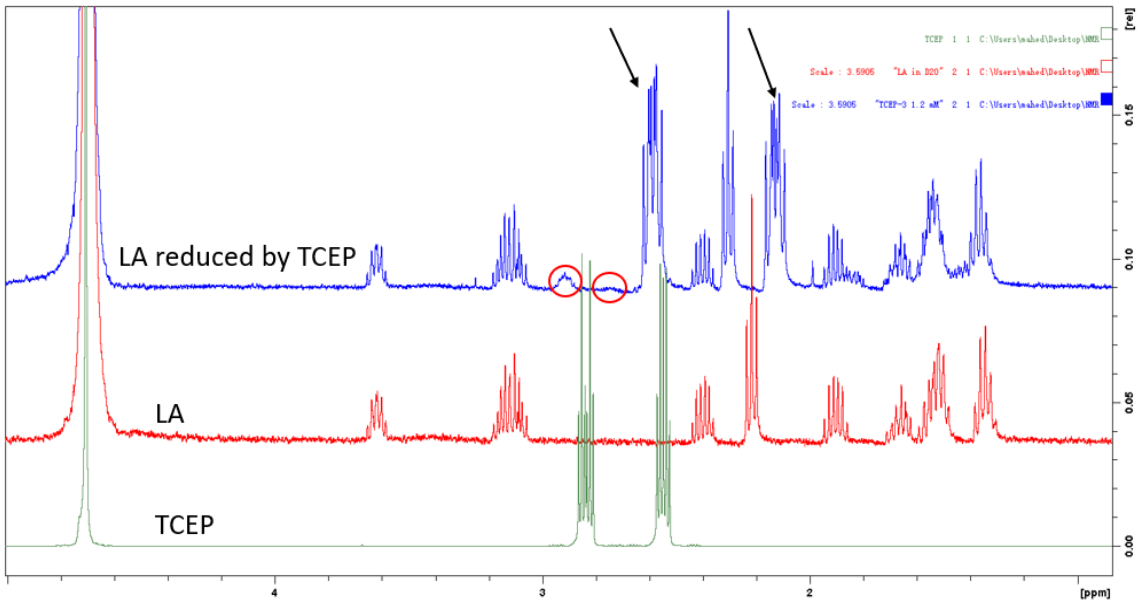

Figure 3-21. The NMR spectrum of LA reduced by TCEP and spectra of TCEP and LA as references. All spectra were taken in D_2O with solvent peak at 4.80ppm. Red circles indicated the existence of DHLA and black arrows indicated oxidized TCEP.

The success of the reduction process was the critical question to be illustrated. Formation of DHLA was demonstrated by the emergence of two new signals at 2.7 and 2.9ppm, labeled by the red circle. These two peaks match well with the reported DHLA signals.[31] The two black arrows indicated the shift to more upfield (low ppm) of TCEP signals. These two peaks match well with the signals of the oxidized form of TCEP.[52] All signals of TCEP were shifted, indicating all TCEP was used up by the LA. It is important to make sure no more TCEP was left in the solution used to anneal the NCs sample because TCEP will decompose the NCs. The control experiment was performed to investigate the reaction between TCEP and NCs. Figure 3-22 shows the absorbance and photoluminescence spectra of the NCs before and after the addition of TCEP.

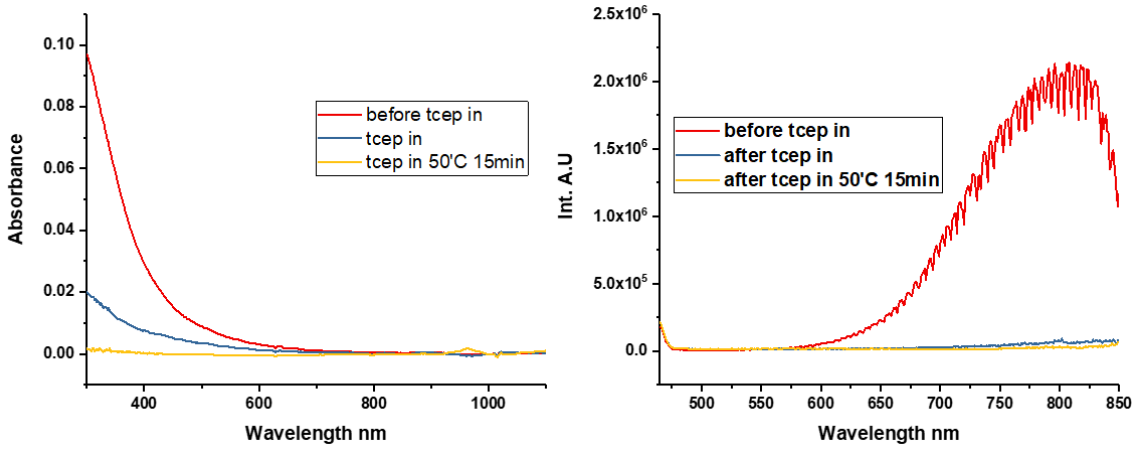

Figure 3-22. Raw data of a) UV-Vis spectra of NCs before and after the addition of TCEP. b) photoluminescence of the NCs before and after the addition of TCEP.

The brown color of the NCs was immediately changed to transparency along with the decrease of the absorbance and emission intensity after the addition of the TCEP. The NCs sample was apparently decomposed by TCEP.

Upon completing the TCEP control experiments, NCs were annealed with disulfide form of LA. There is no change in absorbance and emission during the thermal treatment process. Therefore, the property changes presented next occur due to the reactions of the NCs and DHLA only.

Next, the NCs were annealed following the same procedure as MonoThiols shown above. A reduced solution of LA by TCEP (no purification performed), i.e. DHLA, was used to anneal the molecular-like NCs at 60^{o}C. Absorbance and photoluminescence spectra during the annealed process were recorded shown in Figure 3-23. Photoluminescence intensity of the emission spectra at 800nm peaks is plotted in Figure 3-24 to demonstrate the trend. At around 75 to 90 minutes, the annealed sample showed maximum QE. The process was stopped immediately, and the annealed sample was purified by the ultra-centrifuge method.

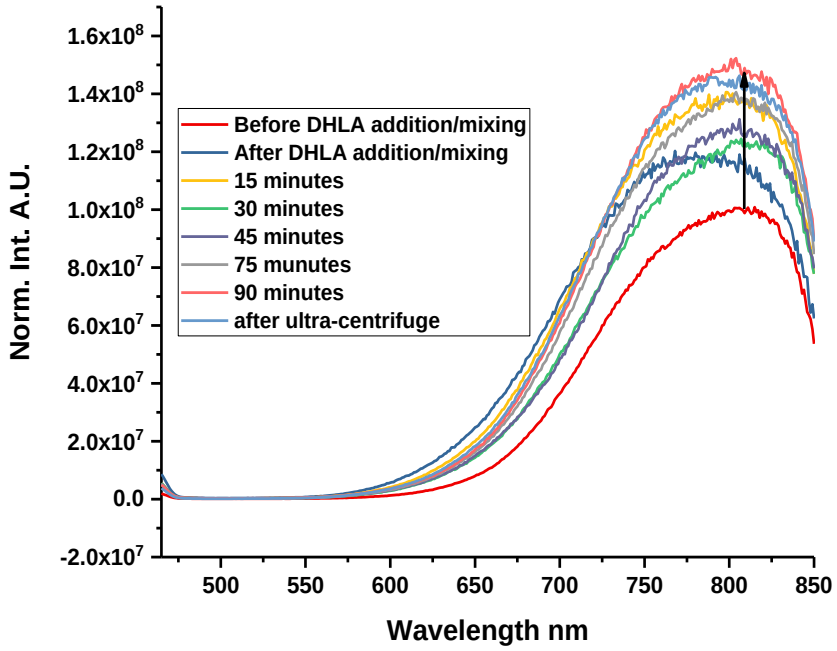

Figure 3-23 Normalized emission spectra of molecular like Au-LA NCs during the annealed process with aqueous DHLA at 60°C. Luminescence spectra were normalized by the absorbance at the excitation wavelength of 400 nm.

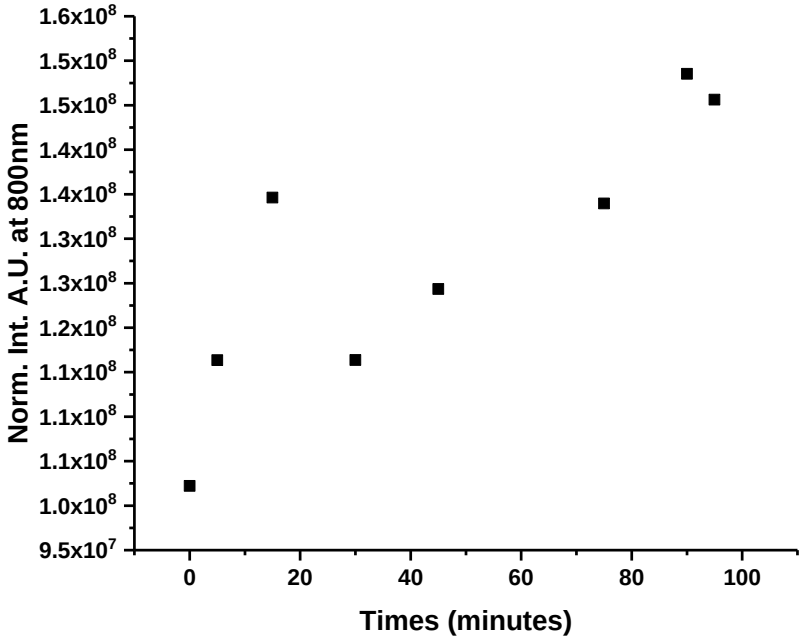

Figure 3-24 Normalized photoluminescence intensity at 800nm during the annealing process. Note in separate measurements (not shown), the emission intensities decrease significantly after longer annealing time.

The Au NCs before annealing had around 10% QE. Almost 2% increase was recorded right after the DHLA was added. The same trend was observed with MonoThiolate annealing process. First, the QE increased than slightly decreased at 30 minutes. After the slight drop, QE increased, reaching maximum at around 90 minutes. The annealed sample was taken out and purified by ultracentrifuge method immediately. After purification, the sample had QE around 15%.

As expected, there is no major changes in NMR and IR spectra because the same ligand was used to anneal the NCs. It is still interesting to find the IR spectra showed no changes before and after annealing. S-H bands at 2500 cm^{-1} did not emerge which indicate there are no free ligands in the final NCs. The results also suggest the oxidized S and unoxidized S remain

unaffected. One of the initial goals of the annealing process is to enhance the purity or monodispersity of the NCs. Both UV-vis and NMR features remain unaffected, which means either the original NCs are already uniform, or the selected thiol:NC ratio is inadequate to induce significant changes. In other words, the observed PL enhancement arise from subtle factors to be resolved. No TCEP signals were obtained in the NMR spectrum which proved the efficacy of the purification method.

There are changes in electrochemiluminescence (ECL) and electrochemistry as shown in the figure 3-25.

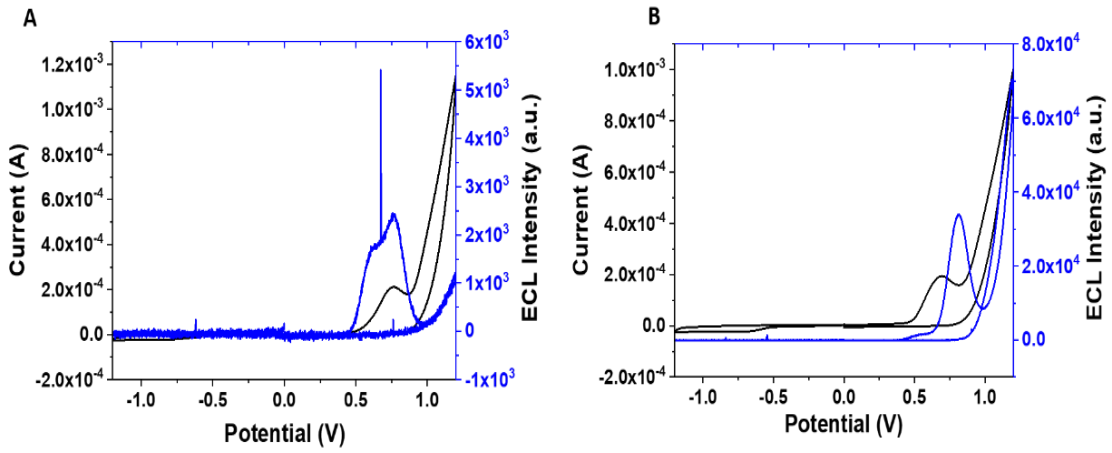

Figure 3-25. CV-ECL of Au-LA (A) and Au-LA annealed by DHLA (B). Data collected with 25 mM HEPES as ECL co-reactants and 0.2 M $NaClO_4$ as supporting electrolyte. The black line is CV, and the blue line is ECL. Potential range is from -1.2 to 1.2 V. Glassy carbon as working electrode, Pt foil as a counter electrode, and Ag/AgCl as a reference electrode.

The black curves showed the ECL signal of the NCs before and after annealing. The ECL is generated by the oxidation of both AuNCs and the coreactant HEPES. After electrode oxidation of one of the HEPES tertiary amine functional group, similar to other ECL coreactants, HEPES undergoes deprotonation and becomes a strong reductant which reacts with the oxidized AuNCs to produce the excited species which emits photon as ECL signal. The annealed sample had

much higher ECL signal. At least a 30-fold increase in ECL intensity was recorded with AuNCs at comparable concentrations. Because the concentration of AuNCs is much lower than HEPES, the current peak at around 0.7V is from HEPES, though the AuNCs also display a weak broad oxidation feature. Optimization of the annealing parameter should be investigated in the future. While the enhancement in ECL by annealing is reproduced, the exact enhancement factor varied (consistently more than ten folds?). Systematic studies on the annealing parameters are needed.

3.5 Conclusion

A new water-soluble Au-LA NCs was synthesized at an optimized ratio of 1.7 moles of LA ligands to every 1 mole of Au salt. The NCs purified by two different purified methods resulted in different luminescence property. A faster purification via ultra-centrifuge resulted in the sample with distinct absorbance bands at 500nm, 590nm, and 680nm. These bands represent different electronic transitions or energy states, which are signatures of a new nanocluster to be fully characterized. In addition to basic electrochemistry and steady-state spectroscopic characterizations, spectroelectrochemistry method was employed to analyze the energetics of this new NCs. After an electrolysis under the potential more positive than the HOMO state/s, the absorbance of the NCs around the three distinct bands changed indicating the change and shift of the related energy states. After a slower purification process via dialysis over days under ambient conditions, specifically exposure to oxygen, gradual oxidation of some sulfur atoms were identified. The photoluminescence of the oxidized sample was enhanced by ten-fold with the tradeoff of diminishment of the distinct absorbance bands. To expedite and better control the partial oxidation of ligands or core-ligand interfacial bonding, the Au-LA Ncs were treated with known amount of excess thiols at elevated temperatures, i.e. annealing. The near IR photoluminescence intensity further increased with the dialyzed sample reaching about 15% QE.

Intriguingly, annealing with the DiThiolate DHLA also improved the ECL of the NCs by at least 30-fold via co-reactant pathway. The reason for the enhancement in ECL has not been understood; future research is needed.

4 SUMMARY

In summary, the work reported in this thesis focuses on the synthesis of Gold-Lipoic nanoparticles within different size regimes, as well as the characterization of their electronic structures and properties. Lipoic acid was selected because of the multidentate capability as a disulfide/dithiolate ligand monolayer to stabilize the gold core and provide aqueous solubility for the relatively larger nanoparticles and smaller nanoclusters. Varying the ratio between gold and Lipoic acid in the synthesis produces different sized nanomaterials and correspondingly the physicochemical properties.

At LA mole ratio smaller than 0.4 compared to Au, the synthetic product was spherical surface plasmon nanoparticles with the plasmonic band at 520 nm. A lower ratio of LA created bigger nanoparticles indicated by the higher plasmonic band intensities. Several synthetic conditions were varied to tune the NPs and related optical and electrochemical properties. FTIR and NMR spectroscopy analysis revealed bonding structures at the core-ligand interactions specifically the gradual oxidation of some ligand sulfur atoms. Electrochemical and spectroelectrochemical methods were used to investigate the energy states and electronic transitions of the NPs. Key energy states were confirmed consistent in aqueous and organic solvents from the major species in the tested Au NPs. Electrolysis of the Au NPs induced detectable changes in the UV-vis absorption spectrum, notably an increase in absorbance around the SP band. Interestingly, upon oxidation at high positive potentials (1.0 & 1.2V), a significant red-shift in the positive differential absorbance band from 600 to 628 nm is observed. The results provide the much needed experimental results of NPs at the transition from larger metallic nanoparticles to smaller non-metallic nanoclusters. Further characterizations and theoretical analysis will be necessary.

At LA mole ratio of 1.7 to Au salt, a new molecular like nanocluster was formed. The NCs purified by different methods yielded different optical features. The ultracentrifuge method resulted in NCs with lower luminescence but contained three distinct bands in the absorbance spectrum, an occurrence which is unique and reported here for the first time. The distinct peaks suggested the monodisperse of the clusters and more importantly a new NC with new energy states. The NCs purified by dialysis experienced longer exposure to oxygen in the synthetic mixture. Gradual oxidization of some ligand sulfur was characterized by FTIR and NMR, giving rise to a tenfold increase in near IR photoluminescence QE. However, absorbance spectra lost those distinct peaks. Specifically, NMR and IR spectra showed the evidence for the bonding of both sulfur to the Au core which restricted the free rotation, as well the oxidation of some inner sulfur atoms in some ligands. In IR spectra, there is no S-H signal at 2500cm^{-1} which indicated that no free LA exist/detectable. The S=O symmetry/asymmetry stretching band indicated the oxidation of the ligand which resulted in the enhancement of QE. Further, the thermal treatment with excess monothiolate and dithiolate ligands enhanced the photoluminescence QE of the NCs from about 7-10% to 15% in dialyzed purification NCs. For the first time for any Au NCs to the best of our knowledge, the ECL intensity was increased at least thirtyfold after the annealing process when dithiolate DHLA was used. Even though the annealing condition process was not fully optimized, the result is very intriguing and needs more future investigation.

REFERENCES

1. Göpel, W., Nanosystems: Molecular machinery, manufacturing and computation. By K. Eric Drexler, J. Wiley & Sons, Chichester, UK 1992, 556 pp., hardcover, £ 19.50, ISBN 0-471-57547-X. *Advanced Materials* **1993,** *5* (11), 865-866.
2. Eustis, S.; El-Sayed, M. A., Why gold nanoparticles are more precious than pretty gold: Noble metal surface plasmon resonance and its enhancement of the radiative and nonradiative properties of nanocrystals of different shapes. *Chemical Society Reviews* **2006,** *35* (3), 209-217.
3. Taniguchi, N., On the Basic Concept of Nano-Technology. *Proc. Intl. Conf. Prod. London, 1974* **1974**.
4. Benelmekki, M., An introduction to nanoparticles and nanotechnology. In *Designing Hybrid Nanoparticles*, Morgan & Claypool Publishers: 2015; pp 1-1-1-14.
5. Ghosh, S. K.; Pal, T., Interparticle Coupling Effect on the Surface Plasmon Resonance of Gold Nanoparticles: From Theory to Applications. *Chemical Reviews* **2007,** *107* (11), 4797-4862.
6. Daniel, M.-C.; Astruc, D., Gold Nanoparticles: Assembly, Supramolecular Chemistry, Quantum-Size-Related Properties, and Applications toward Biology, Catalysis, and Nanotechnology. *Chemical Reviews* **2004,** *104* (1), 293-346.
7. Kawabata, A., Electronic Properties of Fine Metallic Particles. III. E.S.R Absorption Line Shape. *Journal of the Physical Society of Japan* **1970,** *29* (4), 902-911.
8. Jin, R., Quantum sized, thiolate-protected gold nanoclusters. *Nanoscale* **2010,** *2* (3), 343-62.
9. Faraday, M., X. The Bakerian Lecture. —Experimental relations of gold (and other metals) to light. *Philosophical Transactions of the Royal Society of London* **1857,** *147*, 145-181.
10. Mooradian, A., Photoluminescence of Metals. *Physical Review Letters* **1969,** *22* (5), 185-187.
11. Brust, M.; Walker, M.; Bethell, D.; Schiffrin, D. J.; Whyman, R., Synthesis of thiol-derivatised gold nanoparticles in a two-phase Liquid-Liquid system. *Journal of the Chemical Society, Chemical Communications* **1994,** *0* (7), 801-802.
12. Brust, M.; Fink, J.; Bethell, D.; Schiffrin, D. J.; Kiely, C., Synthesis and reactions of functionalised gold nanoparticles. *Journal of the Chemical Society, Chemical Communications* **1995,** (16), 1655-1656.
13. Jao, Y.-C.; Chen, M.-K.; Lin, S.-Y., Enhanced quantum yield of dendrimer-entrapped gold nanodots by a specific ion-pair association and microwave irradiation for bioimaging. *Chemical Communications* **2010,** *46* (15), 2626-2628.
14. Kumara, C.; Dass, A., Au329(SR)84 Nanomolecules: Compositional Assignment of the 76.3 kDa Plasmonic Faradaurates. *Analytical Chemistry* **2014,** *86* (9), 4227-4232.
15. Kumara, C.; Zuo, X.; Ilavsky, J.; Cullen, D.; Dass, A., Atomic Structure of Au329(SR)84 Faradaurate Plasmonic Nanomolecules. *The Journal of Physical Chemistry C* **2015,** *119* (20), 11260-11266.
16. Hu, M.; Chen, J.; Li, Z.-Y.; Au, L.; Hartland, G. V.; Li, X.; Marquez, M.; Xia, Y., Gold nanostructures: engineering their plasmonic properties for biomedical applications. *Chemical Society Reviews* **2006,** *35* (11), 1084-1094.
17. Reynolds, R. A.; Mirkin, C. A.; Letsinger, R. L., Homogeneous, Nanoparticle-Based Quantitative Colorimetric Detection of Oligonucleotides. *Journal of the American Chemical Society* **2000,** *122* (15), 3795-3796.

18. Tessier, P. M.; Velev, O. D.; Kalambur, A. T.; Rabolt, J. F.; Lenhoff, A. M.; Kaler, E. W., Assembly of Gold Nanostructured Films Templated by Colloidal Crystals and Use in Surface-Enhanced Raman Spectroscopy. *Journal of the American Chemical Society* **2000,** *122* (39), 9554-9555.
19. Jin, R.; Zeng, C.; Zhou, M.; Chen, Y., Atomically Precise Colloidal Metal Nanoclusters and Nanoparticles: Fundamentals and Opportunities. *Chem. Rev.* **2016,** *116* (18), 10346-10413.
20. Link, S.; Beeby, A.; FitzGerald, S.; El-Sayed, M. A.; Schaaff, T. G.; Whetten, R. L., Visible to Infrared Luminescence from a 28-Atom Gold Cluster. *The Journal of Physical Chemistry B* **2002,** *106* (13), 3410-3415.
21. Zheng, J.; Zhou, C.; Yu, M.; Liu, J., Different sized luminescent gold nanoparticles. *Nanoscale* **2012,** *4* (14), 4073-4083.
22. Hwang, Y.-N.; Jeong, D. H.; Shin, H. J.; Kim, D.; Jeoung, S. C.; Han, S. H.; Lee, J.-S.; Cho, G., Femtosecond Emission Studies on Gold Nanoparticles. *The Journal of Physical Chemistry B* **2002,** *106* (31), 7581-7584.
23. Wang, G.; Huang, T.; Murray, R. W.; Menard, L.; Nuzzo, R. G., Near-IR Luminescence of Monolayer-Protected Metal Clusters. *Journal of the American Chemical Society* **2005,** *127* (3), 812-813.
24. Huang, T.; Murray, R. W., Visible Luminescence of Water-Soluble Monolayer-Protected Gold Clusters. *The Journal of Physical Chemistry B* **2001,** *105* (50), 12498-12502.
25. Chen, L.-Y.; Wang, C.-W.; Yuan, Z.; Chang, H.-T., Fluorescent Gold Nanoclusters: Recent Advances in Sensing and Imaging. *Analytical Chemistry* **2015,** *87* (1), 216-229.
26. Chakraborty, I.; Pradeep, T., Atomically Precise Clusters of Noble Metals: Emerging Link between Atoms and Nanoparticles. *Chemical Reviews* **2017,** *117* (12), 8208-8271.
27. Packer, L.; Cadenas, E., Lipoic acid: energy metabolism and redox regulation of transcription and cell signaling. *Journal of Clinical Biochemistry and Nutrition* **2010,** *48* (1), 26-32.
28. Reed, L. J.; DeBusk, B. G.; Gunsalus, I. C.; Hornberger, C. S., Crystalline α-Lipoic Acid: A Catalytic Agent Associated with Pyruvate Dehydrogenase. *Science* **1951,** *114* (2952), 93-94.
29. Packer, L.; Cadenas, E., Lipoic acid: energy metabolism and redox regulation of transcription and cell signaling. *Journal of clinical biochemistry and nutrition* **2011,** *48* (1), 26-32.
30. Jiang, J. C., Cecil V.; Kvetny, Maksim M.; Lake, Gabriel J.; Padelford, Jonathan W.; Ahuja, Tarushee; Wang, Gangli, Oxidation at the Core-ligand Interface of Au Lipoic Acid Nanoclusters that Enhances the near IR Luminescence. *The Journal of Physical Chemistry C* **2014,** *Submitted*.
31. Wada, N.; Wakami, H.; Konishi, T.; Matsugo, S., The Degradation and Regeneration of α-Lipoic Acid under the Irradiation of UV Light in the Existence of Homocysteine. *Journal of Clinical Biochemistry and Nutrition* **2009,** *44* (3), 218-222.
32. Tang, Z.; Robinson, D. A.; Bokossa, N.; Xu, B.; Wang, S.; Wang, G., Mixed Dithiolate Durene-DT and Monothiolate Phenylethanethiolate Protected Au130 Nanoparticles with Discrete Core and Core-Ligand Energy States. *Journal of the American Chemical Society* **2011,** *133* (40), 16037-16044.
33. Tang, Z.; Xu, B.; Wu, B.; Robinson, D. A.; Bokossa, N.; Wang, G., Monolayer Reactions of Protected Au Nanoclusters with Monothiol Tiopronin and 2,3-Dithiol Dimercaptopropanesulfonate. *Langmuir* **2011,** *27* (6), 2989-2996.

34. Tang, Z.; Ahuja, T.; Wang, S.; Wang, G., Near infrared luminescence of gold nanoclusters affected by the bonding of 1,4-dithiolate durene and monothiolate phenylethanethiolate. *Nanoscale* **2012,** *4* (14), 4119-4124.
35. Hou, W.; Dasog, M.; Scott, R. W. J., Probing the Relative Stability of Thiolate- and Dithiolate-Protected Au Monolayer-Protected Clusters. *Langmuir* **2009,** *25* (22), 12954-12961.
36. Zhang, S.; Leem, G.; Srisombat, L.-o.; Lee, T. R., Rationally Designed Ligands that Inhibit the Aggregation of Large Gold Nanoparticles in Solution. *Journal of the American Chemical Society* **2007,** *130* (1), 113-120.
37. Tang, Z.; Xu, B.; Wu, B.; Germann, M. W.; Wang, G., Synthesis and Structural Determination of Multidentate 2,3-Dithiol-Stabilized Au Clusters. *Journal of the American Chemical Society* **2010,** *132* (10), 3367-3374.
38. I. Mishchenko, M.; W. Hovenier, J.; D. Travis, L., *Light Scattering by Nonspherical Particles: Theory, Measurements, and Applications*. 2000; p 690.
39. Shang, L.; Azadfar, N.; Stockmar, F.; Send, W.; Trouillet, V.; Bruns, M.; Gerthsen, D.; Nienhaus, G. U., One-pot synthesis of near-infrared fluorescent gold clusters for cellular fluorescence lifetime imaging. *Small* **2011,** *7* (18), 2614-20.
40. Shang, L.; Dong, S.; Nienhaus, G. U., Ultra-small fluorescent metal nanoclusters: Synthesis and biological applications. *Nano Today* **2011,** *6* (4), 401-418.
41. Wu, Z.; Jin, R., On the Ligand's Role in the Fluorescence of Gold Nanoclusters. *Nano Lett.* **2010,** *10* (7), 2568-2573.
42. Conroy, C. V.; Jiang, J.; Zhang, C.; Ahuja, T.; Tang, Z.; Prickett, C. A.; Yang, J. J.; Wang, G., Enhancing near IR luminescence of thiolate Au nanoclusters by thermo treatments and heterogeneous subcellular distributions. *Nanoscale* **2014,** *6* (13), 7416-23.
43. Zhang, J.; Fu, Y.; Conroy, C. V.; Tang, Z.; Li, G.; Zhao, R. Y.; Wang, G., Fluorescence Intensity and Lifetime Cell Imaging with Luminescent Gold Nanoclusters. *The Journal of Physical Chemistry C* **2012,** *116* (50), 26561-26569.
44. Xie, J.; Zheng, Y.; Ying, J. Y., Protein-Directed Synthesis of Highly Fluorescent Gold Nanoclusters. *J. Am. Chem. Soc.* **2009,** *131* (3), 888-889.
45. Padelford, J. W.; Zhou, M.; Chen, Y.; Jin, R.; Wang, G., Electronic Transitions in Highly Symmetric Au130 Nanoclusters by Spectroelectrochemistry and Ultrafast Spectroscopy. *The Journal of Physical Chemistry C* **2017,** *121* (39), 21217-21224.
46. Hartland, G. V., Optical Studies of Dynamics in Noble Metal Nanostructures. *Chemical Reviews* **2011,** *111* (6), 3858-3887.
47. Khlebtsov, N.; Dykman, L., Biodistribution and toxicity of engineered gold nanoparticles: a review of in vitro and in vivo studies. *Chemical Society Reviews* **2011,** *40* (3), 1647-1671.
48. Alkilany, A. M.; Lohse, S. E.; Murphy, C. J., The Gold Standard: Gold Nanoparticle Libraries To Understand the Nano–Bio Interface. *Accounts of Chemical Research* **2013,** *46* (3), 650-661.
49. Burns, J. A.; Butler, J. C.; Moran, J.; Whitesides, G. M., Selective reduction of disulfides by tris(2-carboxyethyl)phosphine. *The Journal of Organic Chemistry* **1991,** *56* (8), 2648-2650.
50. Padelford, J. W., "Characterizing the Optical and Electrochemical Properties of Monolayer-Protected Noble Metal Nanoclusters." Dissertation, Georgia State University, 2018., Characterizing the Optical and Electrochemical Properties of Monolayer-Protected Noble Metal Nanoclusters.

51. Padelford, J. W.; Wang, T.; Wang, G., Enabling Better Electrochemical Activity Studies of H2O-Soluble Au Clusters by Phase Transfer and a Case Study of Lipoic-Acid-Stabilized Au22. *ChemElectroChem* **2016,** *3* (8), 1201-1205.
52. Cumnock, K.; Tully, T.; Cornell, C.; Hutchinson, M.; Gorrell, J.; Skidmore, K.; Chen, Y.; Jacobson, F., Trisulfide Modification Impacts the Reduction Step in Antibody–Drug Conjugation Process. *Bioconjugate Chemistry* **2013,** *24* (7), 1154-1160.
53. Sahyun, M. R. V.; Serpone, N., Photophysics of Thiacarbocyanine Dyes: Relaxation Dynamics in a Homologous Series of Thiacarbocyanines. *The Journal of Physical Chemistry A* **1997,** *101* (51), 9877-9883.

APPENDICES

Appendix A: Chemicals

Tetrachloroauric acid trihydrate ($HAuCl_4 \cdot 3H_2O$, >99.99%), sodium borohydride ($NaBH_4$, 99%), deuterium oxide (D_2O, 99.9%), Sodium perchlorate ($NaClO_4$, 99.9%), Lipoic acid (LA,>99%), Sodium hydroxide (NaOH, >97%), deuterium oxide (D_2O, 99%) were purchased from Sigma-Aldrich and used as received. Potassium phosphate monobasic (KH_2PO_4, ≥99.5%) and potassium phosphate dibasic (K_2HPO_4, ≥99.0%) were purchased from Fluka and used as received. Nanopore water (>18 MΩ.cm) from a Barnstead system was used in all preparations.

Appendix B: Instrumentation and Measurements

UV-Visible absorbance spectra were recorded with a Shimadzu UV-1700 spectrophotometer. Photoluminescence spectra were recorded with a Horiba Jobin-Yvon Fluorolog 311 spectrometer equipped with PMT visible and InGaAs near IR detectors. A Hoya Y-44 long-pass filter was used to collect emission spectra. QE was calculated from the combined detector responses with the corresponding absorbance values ranging 0.05-0.1 at the wavelength of excitation 400 nm. DTTC in methanol was used as standard (QE=21%).[53] NMR 400 MHz spectrometer was used to collect NMR spectra (1D proton and 2D COSY). Infrared spectra were acquired on a PerkinElmer Spectrum 100FT-IR spectrometer. Electrochemical measurements were performed on a CH Instruments (CHI 750C) with Picoamp booster in Faraday Cage. The solution was generally purged over 15-30 mins with Ar prior to electrochemical measurements. The potential of the AgQRE (0.22 V vs. SHE) was calibrated periodically by measuring the ferrocene (Fc+/Fc) redox peak at 0.48 V.